ESAIM: M2AN 53 (2019) 1667–1694
https://doi.org/10.1051/m2an/2019030

ESAIM: Mathematical Modelling and Numerical Analysis
www.esaim-m2an.org

COUPLING NON-CONFORMING DISCRETIZATIONS OF PDES BY SPECTRAL APPROXIMATION OF THE LAGRANGE MULTIPLIER SPACE

Simone Deparis, Antonio Iubatti and Luca Pegolotti*

Abstract. This work focuses on the development of a non-conforming method for the coupling of PDEs based on weakly imposed transmission conditions: the continuity of the global solution is enforced by a finite number of Lagrange multipliers defined over the interfaces of adjacent subdomains. The method falls into the class of primal hybrid methods, which include also the well-known mortar method. Differently from the mortar method, we discretize the space of basis functions on the interface by spectral approximation independently of the discretization of the two adjacent domains. In particular, our approach can be regarded as a specialization of the three-field method in which the spaces used to enforce the continuity of the solution and its conormal derivative across the interface are taken equal. One of the possible choices to approximate the interface variational space – which we consider here – is by Fourier basis functions. As we show in the numerical simulations, the method is well-suited for the coupling of problems defined on globally non-conforming meshes or discretized with basis functions of different polynomial degree in each subdomain. We also investigate the possibility of coupling solutions obtained with incompatible numerical methods, namely the finite element method and isogeometric analysis.

Mathematics Subject Classification. 65N55, 65N60.

Received March 6, 2018. Accepted April 25, 2019.

1. Introduction

In numerical analysis, domain decomposition methods are techniques for the splitting of Partial Differential Equations (PDEs) into smaller and coupled problems defined over subsets of the original domain. The splitting may be motivated by physical reasons, for instance when the subdomains are characterized by different governing equations (*e.g.* in fluid-structure-interaction problems [23]) or by discretization needs, should it be required to employ specific methods – *e.g.* finite element method (FEM) or isogeometric analysis (IGA) – or specific polynomial degrees in certain regions of the domain [45]. Moreover, domain decomposition methods allow the mapping of the subproblems to separate cores [32] and the computation of scalable and efficient parallel preconditioners. These techniques have become so important to the solution of large scale problems on multiprocessors or clusters that, nowadays, the term "domain decomposition" is most commonly used in the context of high performance computing.

Keywords and phrases. Non-conforming method, finite element method, isogeometric analysis.

SCI-SB-SD, Institute of Mathematics, École Polytechnique Fédérale de Lausanne, Station 8, CH-1015 Lausanne, Switzerland.
*Corresponding author: luca.pegolotti@epfl.ch

Domain decomposition methods are typically based either on iterative or direct procedures [3]. In the first class of techniques the continuity on the interfaces of the solution, of its normal derivatives or combinations of the two are strongly imposed. Typically, these methods require solving the problems defined on the subdomains separately multiple times while imposing artificial boundary conditions based on the solutions at the previous iteration. The type of boundary conditions employed on each subdomain is a peculiarity of each algorithm, so that the literature on the topic commonly refers to the Dirichlet–Dirichlet algorithm, the Dirichlet–Neumann algorithm, and so on; see *e.g.* [45] for details. These strategies allow reducing the size of the linear systems to be solved and, most importantly, to compute the solution in each subdomain in parallel.

In this paper, we present an approach belonging to the class of direct procedures in which the continuity conditions (often called *transmission conditions*) are weakly imposed through the use of suitable Lagrange multipliers. Our method is applied to PDEs written in primal hybrid formulation, and for this reason it shares some of the features of the well-known mortar method [6, 7]. This was originally proposed to solve PDEs by combining spectral elements and finite elements, or by combining finite element spaces with different polynomial degrees, in non overlapping portions of the domain [38]. Since then, the mortar method has become the non-conforming method of choice in many areas of computational science and engineering, for example in contact mechanics [36], solid mechanics [35], fluid mechanics [26] and fluid-structure interaction problems [33]; see also [5, 29, 34]. The implementation of the mortar method is not straightforward, as the algorithm is based on L^2-projections of the traces of functional spaces defined on a group subdomains – the masters – onto the interfaces of the adjacent ones – the slaves. INTERNODES [25], a recently developed method for the treatment of non-conforming meshes, overcomes this issue by treating the transmission conditions with the interpolation of basis functions of the master domains onto the interfaces of the slaves.

As in the mortar method, our approach is based on the idea that the global problem can be subdivided into a set of smaller problems coupled with weak conditions relying on basis functions defined on the interfaces. In the mortar method, such basis functions are obtained from the trace space of the adjacent slave domains. This choice is convenient from the analysis standpoint but makes the implementation of the method cumbersome. Another drawback is that the final solution is dependent on the choice of master and slave domains. The originality of our method is to consider basis functions on the interfaces which are completely independent of the discretization of the neighboring domains: in this paper, we employ spectral basis functions (specifically, Fourier basis functions). The same choice has been recently adopted in [10] in the context of IGA for the simulation of electric machines. However, we also consider Fourier basis functions which are not periodic nor orthogonal by introducing an orthonormalization step and we provide a link with theoretical convergence results. The advantage of the approach we present is that the resulting global solution is not dependent on the classification of master and slave domains, which in fact is not required. Moreover, the accuracy of the coupling of solutions at the interfaces is easily tuned by varying the number of basis functions on the common boundary. Our approach can be interpreted as a specialization of the three-field method [15], where the space of the three Lagrange multipliers used to weakly impose the continuity of the solution is (*a priori*) independent of the spaces defined on the adjacent domains. As the functional spaces in the subdomains are mutually independent, our choice of basis functions is well-suited for the coupling of solutions obtained on non-conforming (at the interfaces) meshes, with finite element spaces with different polynomial degrees, or with different numerical methods, *e.g.* FEM, spectral element method, or IGA. In this paper, we specifically consider the coupling of FEM and IGA, although one of our aims in future works is the consider the coupling of reduced basis solutions by a small number of basis functions on the interfaces, so that the coupling itself can be considered *reduced*.

The paper is structured as follows. In Section 2, we present the method on an elliptic problem defined over a domain partitioned into two regions. Section 3 focuses on the discretization of the weak formulation derived in Section 2. In Section 4, we briefly compare our method with other non-conforming methods, namely the mortar method, INTERNODES, and the three-field method, and focus on the similarities and peculiarities with respect to our approach. In Section 5 we address the matter of the stability of the method, which is strictly related to the inf-sup condition. In Section 6, the method is used to solve two dimensional and three-dimensional benchmark problems: we consider the Poisson problem approximated with FEM on two subdomains (Sect. 6.2) and the

Navier–Stokes equations on three subdomains (Sect. 6.3), numerically solved by employing FEM (Sect. 6.3.1) and FEM coupled with IGA (Sect. 6.3.2). Finally, in Section 7 some conclusions are drawn.

1.1. Notation

The notation adopted in this paper is standard and commonly found in the literature; see *e.g.* [39]. Given a generic open and bounded domain Ω embedded in $\mathbb{R}^d$, we define, for all $\varphi, \psi : \Omega \to \mathbb{R}$ and all $\boldsymbol{\varphi}, \boldsymbol{\psi} : \Omega \to \mathbb{R}^d$

$$(\varphi, \psi)_\Omega := \int_\Omega \varphi\psi \, \mathrm{d}\mathbf{x}, \quad (\boldsymbol{\varphi}, \boldsymbol{\psi})_\Omega := \int_\Omega \boldsymbol{\varphi} \cdot \boldsymbol{\psi} \, \mathrm{d}\mathbf{x},$$

and consider the following Hilbert spaces

$$\begin{aligned} L^2(\Omega) &:= \{\varphi : \Omega \mapsto \mathbb{R} : (\varphi, \varphi)_\Omega \ < \infty\}, \\ H^1(\Omega) &:= \{\varphi \in L^2(\Omega) : \nabla\varphi \in [L^2(\Omega)]^d\}, \\ H(\mathrm{div}; \Omega) &:= \{\boldsymbol{\phi} \in [L^2(\Omega)]^d : \mathrm{div}\boldsymbol{\phi} \in L^2(\Omega)\}, \end{aligned}$$

with the associated norms

$$\begin{aligned} \|\varphi\|^2_{L^2(\Omega)} &:= (\varphi, \varphi)_\Omega, \\ \|\varphi\|^2_{H^1(\Omega)} &:= (\varphi, \varphi)_\Omega + (\nabla\varphi, \nabla\varphi)_\Omega, \\ \|\boldsymbol{\phi}\|^2_{H(\mathrm{div};\Omega)} &:= (\boldsymbol{\phi}, \boldsymbol{\phi})_\Omega + (\mathrm{div}\boldsymbol{\phi}, \mathrm{div}\boldsymbol{\phi})_\Omega. \end{aligned}$$

Given a measurable set $\Sigma \subseteq \partial\Omega$ (where $\partial\Omega$ denotes the boundary of Ω), we also define

$$H^1_\Sigma(\Omega) := \{\varphi \in H^1(\Omega) : \ \varphi = 0 \text{ on } \Sigma\}.$$

If $\Sigma \equiv \partial\Omega$, $H^1_\Sigma(\Omega)$ is equal to $H^1_0(\Omega)$.

Under the assumption of sufficient regularity of Σ, there exists a unique linear and continuous application $\gamma_\Sigma : H^1(\Omega) \mapsto L^2(\Sigma)$ called trace operator [37, 42] such that $\gamma_\Sigma\varphi = \varphi|_\Sigma$ for all $\varphi \in H^1(\Omega) \cap C^0(\bar{\Omega})$, having indicated with $C^0(\bar{\Omega})$ the space of continuous functions over the closure of Ω. The range of such operator is denoted $H^{1/2}(\Sigma) \subset L^2(\Sigma)$. We recall that

$$\|\eta\|_{H^{1/2}(\Sigma)} := \inf_{\substack{\varphi \in H^1(\Omega) \\ \varphi|_\Sigma = \eta}} \|\varphi\|_{H^1(\Omega)}$$

is a norm for $H^{1/2}(\Sigma)$ [11].

For each linear Hilbert space $\mathcal{H}$, we denote $\mathcal{H}'$ the space of linear and bounded functionals on $\mathcal{H}$, namely its dual space. In particular, we adopt the notation $H^{-1}(\Omega) := (H^1(\Omega))'$ and $H^{-1/2}(\Sigma) := (H^{1/2}(\Sigma))'$. The action of an element of the dual space $\xi \in \mathcal{H}'$ on an element of the Hilbert space $\varphi \in \mathcal{H}$ is indicated $\langle \xi, \varphi \rangle_{\mathcal{H}'}$ or simply $\langle \xi, \varphi \rangle$ whenever ambiguity does not arise. Furthermore, we will simply indicate $\langle \xi, \varphi \rangle_\Sigma$ the duality in $H^{-1/2}(\Sigma)$. We note that, for $\varphi \in H^1(\Omega)$, we will adopt the abuse of notation $\langle \xi, \varphi \rangle_\Sigma$ with $\xi \in H^{-1/2}(\Sigma)$ to indicate the duality of ξ with the trace of φ on Σ. Even though not mathematically rigorous, this notation is commonly used in the literature.

2. Theory of primal hybrid methods

In this section, we recall the theory of primal hybrid methods for the solution of PDEs. These approaches are based on the *primal hybrid principle* [40], according to which the continuity across subdomains is weakened by means of Lagrange multipliers. We refer the reader to [1, 4, 9] for the theory of primal hybrid methods. Here, we recall the main ideas by following the presentation in [11]. We also restrict ourselves to partitions comprising

only two subdomains; however – as we shall see in Section 3.1 – the method extends to an arbitrary number of subdomains.

We are interested in solving a generic PDE described by a second order elliptic operator on an open and bounded domain Ω with homogeneous Dirichlet boundary conditions on $\partial\Omega$. Specifically, we assume that $a(\varphi,\psi)$ for $\varphi,\psi \in H^1(\Omega)$ is the bilinear form corresponding to the elliptic operator and f is a given forcing term; we consider problems whose weak formulation can be written as:

(W1) *given* $f \in H^{-1}(\Omega)$*, find* $u \in H^1_0(\Omega)$*, such that*

$$a(u,v) = \langle f, v\rangle \quad \forall v \in H^1_0(\Omega). \tag{2.1}$$

In the sequel, we will use the Poisson problem

$$-\Delta u = f \quad \text{in } \Omega \tag{2.2}$$

with homogeneous Dirichlet boundary conditions (*i.e.* $u = 0$ on $\partial\Omega$) as representative of this class of problems. In this specific case, $a(\varphi,\psi) = (\nabla\varphi, \nabla\psi)_\Omega$.

Let us assume that the domain Ω can be partitioned into two non-overlapping open and bounded domains, such that $\Omega = \Omega_1 \cup \Omega_2$ and $\Omega_1 \cap \Omega_2 = \emptyset$; we denote Γ the interface between the two domains, *i.e.* $\Gamma = \overline{\Omega}_1 \cap \overline{\Omega}_2$. Our goal is to solve, rather than the global problem W1, two local and coupled problems defined on the partitions Ω_i, such that the global solution can be constructed by combining the solutions of the local problems. To this end, let us introduce for $i = 1, 2$ the functional spaces $\mathcal{X}^{(i)} = H^1_{\partial\Omega\cap\partial\Omega_i}(\Omega_i)$ and

$$\mathcal{X} := \{\varphi \in L^2(\Omega) : \varphi|_{\Omega_i} \in \mathcal{X}^{(i)} \text{ for } i = 1, 2\},$$

which is a Hilbert space when endowed with the (broken) norm

$$\|\varphi\|^2_{\mathcal{X}} := \sum_{i=1}^{2} \|\varphi|_{\Omega_i}\|^2_{H^1(\Omega_i)}.$$

The space $H^1_0(\Omega)$ is characterized as a subspace of $\mathcal{X}$ under suitable conditions [11] which we will state in the following Lemma and motivate in its proof. We remark that an analogous result is presented in [9].

Proposition 2.1 ([9], *cf.* Prop. 2.1.1)**.**

$$H^1_0(\Omega) \equiv \widetilde{\mathcal{V}} := \{\varphi \in \mathcal{X} : \sum_{i=1}^{2} \langle \boldsymbol{\phi}\cdot\boldsymbol{n}_i, \varphi\rangle_{\partial\Omega_i} = 0 \quad \forall \boldsymbol{\phi} \in H(\mathrm{div};\Omega)\},$$

where $\boldsymbol{n}_i$ *is the outward unit vector normal to* $\partial\Omega_i$*.*

Proof. Firstly, let us recall that for any $\boldsymbol{\phi} \in H(\mathrm{div};\Omega)$ and for $i = 1, 2$, Green's formula gives Lemma 2.1.1 from [9]

$$\int_{\Omega_i} (\nabla\varphi\cdot\boldsymbol{\phi} + \varphi \mathrm{div}\boldsymbol{\phi})\, \mathrm{d}\mathbf{x} = \langle \boldsymbol{\phi}\cdot\mathbf{n}_i, \varphi\rangle_{\partial\Omega_i} \quad \forall\varphi \in \mathcal{X}. \tag{2.3}$$

Equation (2.3) implies that, since the left hand side is bounded, the duality of $\boldsymbol{\phi}\cdot\mathbf{n}_i \in H^{-1/2}(\partial\Omega_i)$ on the trace of $\varphi|_{\Omega_i}$ is well-defined.

Clearly $\widetilde{\mathcal{V}} \subset H^1_0(\Omega)$, because for all $\varphi \in \widetilde{\mathcal{V}} \subset L^2(\Omega)$

$$\int_\Omega |\nabla\varphi|^2\, \mathrm{d}\mathbf{x} = \sum_{i=1}^{2} \int_{\Omega_i} |\nabla\varphi|^2\, \mathrm{d}\mathbf{x} < \infty,$$

and $\varphi = 0$ on $\partial\Omega$ in $H^{1/2}(\partial\Omega)$. Let us show the other inclusion. For every $\varphi \in H_0^1(\Omega)$, it holds that $\varphi \in L^2(\Omega)$ and $\varphi|_{\Omega_i} \in \mathcal{X}^{(i)}$ for $i = 1, 2$, which implies that $H_0^1(\Omega) \subset \mathcal{X}$. Moreover, by applying Green's formula as in equation (2.3), we find, for all $\boldsymbol{\phi} \in H(\mathrm{div}; \Omega)$,

$$\sum_{i=1}^{2} \langle \boldsymbol{\phi} \cdot \mathbf{n}_i, \varphi \rangle_{\partial\Omega_i} = \sum_{i=1}^{2} \int_{\Omega_i} (\nabla\varphi \cdot \boldsymbol{\phi} + \varphi \mathrm{div}\boldsymbol{\phi}) \, \mathrm{d}\mathbf{x} = \int_{\Omega} (\nabla\varphi \cdot \boldsymbol{\phi} + \varphi \mathrm{div}\boldsymbol{\phi}) \, \mathrm{d}\mathbf{x} = \langle \boldsymbol{\phi} \cdot \mathbf{n}, \varphi \rangle_{\partial\Omega} = 0, \tag{2.4}$$

where the last equality comes from the fact that φ has null trace on the boundary $\partial\Omega$. Since equation (2.4) shows that $H_0^1(\Omega) \subset \widetilde{\mathcal{V}}$, it must be $H_0^1(\Omega) \equiv \widetilde{\mathcal{V}}$. □

Remark 2.2. Proposition 2.1 must be modified if $\partial\Omega = \Gamma_D \cup \Gamma_N$ and if the PDE is equipped with homogeneous Dirichlet conditions on Γ_D and Neumann conditions on Γ_N. Following [9], let us introduce the space

$$H_{\Gamma_N}(\mathrm{div}; \Omega) := \{\boldsymbol{\phi} \in H(\mathrm{div}; \Omega) : \langle \boldsymbol{\phi} \cdot \mathbf{n}, v \rangle_{\partial\Omega} = 0 \quad \forall v \in H^1_{\Gamma_D}(\Omega)\},$$

where $\mathbf{n}$ is the outward unit vector normal to $\partial\Omega$. Then

$$H_0^1(\Omega) \equiv \overset{\circ}{\mathcal{V}} := \{\varphi \in \mathcal{X} : \sum_{i=1}^{2} \langle \boldsymbol{\phi} \cdot \mathbf{n}_i, \varphi \rangle_{\partial\Omega_i} = 0 \quad \forall \boldsymbol{\phi} \in H_{\Gamma_N}(\mathrm{div}; \Omega)\}$$

is a characterization of $H_0^1(\Omega)$.

The condition $\sum_{i=1}^{2} \langle \boldsymbol{\phi} \cdot \mathbf{n}_i, \varphi \rangle_{\partial\Omega_i} = 0$ for each $\boldsymbol{\phi} \in H(\mathrm{div}; \Omega)$ is global, in the sense that it involves the trace of $\varphi|_{\Omega_i}$ on the whole $\partial\Omega_i$, even though it essentially constrains the restrictions of φ to Ω_1 and Ω_2 to have the same trace at the common interface Γ. Unfortunately, splitting the dualities into two parts corresponding to Γ and $\partial\Omega \setminus \Gamma$ is not allowed, as the restrictions of the traces to portions of $\partial\Omega_i$ can lead to unbounded dualities. To overcome this issue, we introduce

$$H_{00}^{1/2}(\Gamma_i) := \{\eta \in H^{1/2}(\Gamma_i) : E_0^{(i)}\eta \in H^{1/2}(\partial\Omega_i)\},$$

with norm

$$\|\eta\|_{H_{00}^{1/2}(\Gamma_i)} := \|E_0^{(i)}\eta\|_{H^{1/2}(\partial\Omega_i)},$$

where $E_0^{(i)}\eta$ is the trivial extension by zero of η to the whole boundary of $\partial\Omega_i$ and $\Gamma_i = \partial\Omega_i \setminus \partial\Omega$. In the following, we will consider $H_{00}^{1/2}(\Gamma) := H_{00}^{1/2}(\Gamma_1) \cap H_{00}^{1/2}(\Gamma_2)$. Let us define the spaces

$$\mathcal{X}_{00} := \{\varphi \in \mathcal{X} : [\varphi]_\Gamma \in H_{00}^{1/2}(\Gamma)\},$$

where $[\varphi]_\Gamma$ denotes by our convention the difference of the traces of $\varphi|_{\Omega_2}$ and $\varphi|_{\Omega_1}$ on Γ, and

$$\Lambda := H_{00}^{-1/2}(\Gamma), \tag{2.5}$$

with norm

$$\|\eta\|_\Lambda := \|\eta\|_{H_{00}^{-1/2}(\Gamma_1)} + \|\eta\|_{H_{00}^{-1/2}(\Gamma_2)}.$$

Furthermore, we introduce the bilinear form

$$b(\varphi, \xi) := \langle \xi, [\varphi]_\Gamma \rangle_\Lambda$$

for $\varphi \in \mathcal{X}_{00}$ and $\xi \in \Lambda$. It can be easily verified [11] that another characterization of $H_0^1(\Omega)$ analogous to that in Proposition 2.1 is given by

$$H_0^1(\Omega) \equiv \mathcal{V} := \{\varphi \in \mathcal{X}_{00} : b(\varphi, \xi) = 0 \quad \forall \xi \in \Lambda\}. \tag{2.6}$$

In the sequel, we will use the letter $\mathcal{V}$ to refer to $H_0^1(\Omega)$.

We are now ready to state the primal hybrid formulation of the original weak formulation W1. We remark that, whenever applied to functions of $\mathcal{X}$, the bilinear form $a(\cdot,\cdot)$ is to be intended as the sum of the bilinear forms restricted to the two subdomains.

(W2) *given $f \in H^{-1}(\Omega)$, find $u \in \mathcal{X}_{00}$ and $\lambda \in \Lambda$ such that*

$$\begin{aligned} a(u,v) + b(v,\lambda) &= \langle f, v\rangle \quad && \forall v \in \mathcal{X}_{00}, \\ b(u,\eta) &= 0 && \forall \eta \in \Lambda. \end{aligned} \tag{2.7}$$

Proposition 2.3. *If $u \in \mathcal{V}$ is a solution of W1 and there exists $\lambda \in \Lambda$ such that*

$$b(v,\lambda) = \langle f, v\rangle - a(u,v) \quad \forall v \in \mathcal{X}_{00}, \tag{2.8}$$

then $(u,\lambda) \in \mathcal{X}_{00} \times \Lambda$ is a solution of W2. On the other hand, if $(u,\lambda) \in \mathcal{X}_{00} \times \Lambda$ is a solution of W2, then $u \in \mathcal{V}$ and u is a solution of W1.

Proof. Let $u \in \mathcal{V}$ be a solution of W1, then $u \in \mathcal{X}_{00}$ and the second condition in equation (2.7) is satisfied because of the definition (2.6). The first condition in equation (2.7) is satisfied when choosing $\lambda \in \Lambda$ such that equation (2.8) is verified. Conversely, if $(u,\lambda) \in \mathcal{X}_{00} \times \Lambda$ is a solution for W2, then $u \in \mathcal{V}$ because of the second condition in equation (2.7). Moreover, for each $v \in \mathcal{V}$, $b(v,\xi) = 0$ for all $\xi \in \Lambda$ and, in particular, for $\xi = \lambda$, and the first condition in equation (2.7) becomes equation (2.1). □

Remark 2.4. If we consider the Poisson equation (2.2), then equation (2.8) is verified by taking $\boldsymbol{\phi} = -\nabla u$ and by choosing $\lambda \in \Lambda$ such that $\boldsymbol{\phi} \cdot \mathbf{n}_1 = \lambda$, $\mathbf{n}_1$ being the outward unit vector normal to $\partial\Omega_1$. Indeed, by using integration by parts we find, for all $v \in \mathcal{X}_{00}$,

$$\begin{aligned} b(v,\lambda) = \langle \boldsymbol{\phi}\cdot\mathbf{n}_1, [v]_\Gamma\rangle_\Lambda &= -\sum_{i=1}^{2} \int_\Gamma \nabla u \cdot \mathbf{n}_i v \, \mathrm{d}\mathbf{s} \\ &= \sum_{i=1}^{2} \left(\int_{\Omega_i} f v \, \mathrm{d}\mathbf{x} - \int_{\Omega_i} \nabla u \cdot \nabla v \, \mathrm{d}\mathbf{x} \right) = \langle f, v\rangle - a(u,v), \end{aligned}$$

where we used the fact that $\mathbf{n}_1 = -\mathbf{n}_2$. Note that, if we defined the jump across the interface of a function $\varphi \in \mathcal{X}_{00}$ as the difference of the traces on Γ of $\varphi|_{\Omega_1}$ and $\varphi|_{\Omega_2}$, then $\boldsymbol{\phi}\cdot\mathbf{n}_2 = \lambda$. Hence, the Lagrange multiplier in equation (2.7) plays the role of the normal derivative of u at the interface Γ [47], with the direction of the normal at the interface being determined by the definition of the jump.

3. Discretization of the primal hybrid formulation

We now consider the discretization of the weak formulation W2. We take two arbitrary finite dimensional functional spaces $\mathcal{X}^{h,(1)} \subset \mathcal{X}^{(1)}$ and $\mathcal{X}^{h,(2)} \subset \mathcal{X}^{(2)}$ spanned by two sets of basis functions $\varphi_i^{(1)} \in \mathcal{X}^{(1)}$ (with $i = 1, \dots, n_{\mathrm{bf}}^{(1)}$) and $\varphi_i^{(2)} \in \mathcal{X}^{(2)}$ (with $i = 1, \dots, n_{\mathrm{bf}}^{(2)}$) respectively. We assume that functions in $\mathcal{X}^{h,(1)}$ and $\mathcal{X}^{h,(2)}$ can be trivially extended by zero in the other domain and that such extension belong to $\mathcal{X}_{00}$. The discrete version of the global space $\mathcal{X}_{00}$ is consequently obtained by considering the space $\mathcal{X}^h \subset \mathcal{X}_{00}$ of dimension $\dim(\mathcal{X}^h) = n_{\mathrm{bf}} = n_{\mathrm{bf}}^{(1)} + n_{\mathrm{bf}}^{(2)}$ and spanned by the basis functions

$$\{\varphi_i\}_{i=1}^{n_{\mathrm{bf}}} = \{\varphi_i^{(1)}\}_{i=1}^{n_{\mathrm{bf}}^{(1)}} \cup \{\varphi_i^{(2)}\}_{i=1}^{n_{\mathrm{bf}}^{(2)}}.$$

The solution can be then approximated as $u \approx u^h = \sum_{i=1}^{n_{\mathrm{bf}}} u_i \varphi_i$. In the numerical applications in Section 6, we will consider standard finite element Lagrangian basis functions and B-Splines basis functions for the discretization of the spaces defined above; in this section we consider – to fix our ideas – the case in which FEM is

employed. The finite element basis functions are built over suitable triangulations $\mathcal{T}^{h,(1)}$ and $\mathcal{T}^{h,(2)}$ of Ω_1 and Ω_2 respectively; we will always assume that such triangulations meet standard regularity requirements [39], but we do not require the conformity of the global mesh $\mathcal{T}^h = \mathcal{T}^{h,(1)} \cup \mathcal{T}^{h,(2)}$. We define conforming meshes those meshes for which the intersection of two elements is either null, a vertex or a whole edge; in non-conforming meshes, on the contrary, two elements can also share portions of their edges. The discretization parameter h is generic and defines a family of discretized spaces; when using finite elements, for example, h refers to the maximum edge length of an element – often called mesh size – in the triangulations of Ω_1 and Ω_2. More generally, h could be also considered a characteristic of the single subdomain, since – as we already mentioned – the discretizations in Ω_1 and Ω_2 are independent one of the other and could be obtained from different discretization methods.

Our proposition is to discretize Λ as Λ^δ by using a set of basis functions $\xi_i \in \Lambda$, such that $\lambda \in \Lambda$ is approximated as $\lambda \approx \lambda^\delta = \sum_{i=1}^{n_\Gamma} \lambda_i \xi_i$. We remark that we characterize the refinement levels for $\mathcal{X}^{h,(1)}$, $\mathcal{X}^{h,(2)}$ and Λ^δ with different discretization parameters h and δ: this is to indicate that the discretization of Λ is indeed independent of the discretization on Ω_1 and Ω_2. For instance, in the two dimensional case, a suitable choice would consist of choosing as ξ_i the basis functions associated to the low-frequencies of the Fourier basis defined on the common interface Γ, and the accuracy of the discretization of Λ^δ can be increased independently of h by adding Fourier basis functions to the set ξ_i. In the numerical simulations of Section 6 we will follow this approach. Alternative possibilities for the discretization of the Lagrange multiplier space include other spectral basis functions, such as *e.g.* Legendre or Chebyshev polynomials.

The discrete space for the approximation of $\mathcal{V}$ is then defined as

$$\mathcal{V}^{h,\delta} := \{\varphi^h \in \mathcal{X}^h : b(\varphi^h, \xi^\delta) = 0 \quad \forall \xi^\delta \in \Lambda^\delta\},$$

Remark 3.1. $\mathcal{V}^{h,\delta}$ is not a subspace of $\mathcal{V}$. As a matter of fact, if Λ^δ is not equal to Λ, then there may exist $\xi \in \Lambda$, $\xi \notin \Lambda^\delta$ such that $b(\varphi^h, \xi) \neq 0$ for some $\varphi^h \in \mathcal{V}^{h,\delta}$, and therefore $\varphi^h \notin \mathcal{V}$. If we replaced $\mathcal{V}$ by $\mathcal{V}^{h,\delta}$ in W1, we would obtain a *non-conforming method*, *i.e.* a numerical method in which the discretized search space is not contained into the continuous search space. The generalized version of Céa's lemma [18] for this family of methods is Strang's second lemma [19], which states that the solution u^h of the discretized version of W1 satisfies

$$\|u - u^h\|_{\mathcal{V}^{h,\delta}} \leq C \left(\inf_{v^h \in \mathcal{V}^{h,\delta}} \|u - v^h\|_{\mathcal{V}^{h,\delta}} + \sup_{w^h \in \mathcal{V}^{h,\delta}} \frac{|a(u, w^h) - \langle f, w^h \rangle|}{\|w^h\|_{\mathcal{V}^{h,\delta}}} \right), \tag{3.1}$$

where $C > 0$ and $\|\cdot\|_{\mathcal{V}^{h,\delta}}$ is a norm for $\mathcal{V}^{h,\delta}$. Note that the consistency error – *i.e.* the second term of the right hand side in equation (3.1) – is identically zero for each $w^h \in \mathcal{V}^{h,\delta}$ if $\mathcal{V}^{h,\delta} \subset \mathcal{V}$ because u is a solution of W1.

The discretization of W2 is simply obtained by replacing the continuous functional spaces with their discrete counterparts, namely:

(W3) *given* $f \in H^{-1}(\Omega)$, *find* $u^h \in \mathcal{X}^h$ *and* $\lambda^\delta \in \Lambda^\delta$ *such that*

$$\begin{aligned} a(u^h, v^h) + b(v^h, \lambda^\delta) &= \langle f, v^h \rangle \quad \forall v^h \in \mathcal{X}^h, \\ b(u^h, \eta^\delta) &= 0 \qquad\qquad\quad \forall \eta^\delta \in \Lambda^\delta. \end{aligned} \tag{3.2}$$

By expanding u^h and λ^δ on their respective bases, equation (3.2) can be rewritten in system form as

$$\begin{bmatrix} A & B^T \\ B & 0 \end{bmatrix} \begin{bmatrix} \mathbf{u} \\ \boldsymbol{\lambda} \end{bmatrix} = \begin{bmatrix} \mathbf{f} \\ \mathbf{0} \end{bmatrix}, \tag{3.3}$$

where $A_{ij} = a(\varphi_j, \varphi_i)$, $B_{ij} = b(\varphi_j, \xi_i)$, $\mathbf{u}_i = u_i$, $\boldsymbol{\lambda} = \lambda_i$ and $\mathbf{f}_i = \langle f, \varphi_i \rangle$. By arranging the basis functions φ_n and the degrees of freedom such that all the basis functions corresponding to Ω_1 come before those of Ω_2,

system (3.3) can be written as

$$\begin{bmatrix} A_1 & 0 & -B_1^T \\ 0 & A_2 & B_2^T \\ -B_1 & B_2 & 0 \end{bmatrix} \begin{bmatrix} \mathbf{u}_1 \\ \mathbf{u}_2 \\ \boldsymbol{\lambda} \end{bmatrix} = \begin{bmatrix} \mathbf{f}_1 \\ \mathbf{f}_2 \\ \mathbf{0} \end{bmatrix},$$

where $(B_1)_{ij} = \int_\Gamma \varphi_j^{(1)} \xi_i \, \mathrm{d}\mathbf{s}$ and $(B_2)_{ij} = \int_\Gamma \varphi_j^{(2)} \xi_i \, \mathrm{d}\mathbf{s}$ are coupling matrices. Clearly, B_1 and B_2 are likely to be sparse if the basis functions internal to the subdomains have compact support, as the integrals are equal to zero if $\varphi_j^{(1)}$ and $\varphi_j^{(2)}$ vanish on Γ.

In this paper, the computation of the coupling matrices is performed by numerically integrating by Gauss quadrature rules the integrals. Let us consider for instance the case of B_1 in the two dimensional case. The triangulation $\mathcal{T}^{h,(1)}$ induces on Γ a partition into $n_{\mathrm{el},\Gamma}^{(1)}$ elements, *i.e.* $\Gamma = \bigcup_{i=1}^{n_{\mathrm{el},\Gamma}^{(1)}} E_i^{(1)}$. Given a Gauss quadrature rule of order $2q-1$, the approximation of each term of B_1 is computed as

$$(B_1)_{mn} = \int_\Gamma \varphi_n^{(1)} \xi_m \, \mathrm{d}\mathbf{s} = \sum_{i=1}^{n_{\mathrm{el},\Gamma}^{(1)}} \int_\Gamma \varphi_n^{(1)} \xi_m \, \mathrm{d}\mathbf{s} \approx \sum_{i=1}^{n_{\mathrm{el},\Gamma}^{(1)}} \sum_{j=1}^{q} |\det(J_i)| \varphi_n^{(1)}(\phi_i(\mathbf{x}_j^{\mathrm{gq}})) \xi_m(\phi_i(\mathbf{x}_j^{\mathrm{gq}})) \omega_j, \tag{3.4}$$

where $\det(J_i)$ is the determinant of the Jacobian of the map $\phi_i : E_i^{(1)} \to (-1,1)$ from $E_i^{(1)}$ to the reference interval $(-1,1)$, $\mathbf{x}_j^{\mathrm{gq}}$ is the jth Gauss quadrature node in $(-1,1)$ and ω_j is the associated weight. As it is evident from equation (3.4), in order to compute the approximation of B_1 it is sufficient being able to evaluate the product $\varphi_n^{(1)}(\phi_i(\mathbf{x}_j^{\mathrm{gq}}))\xi_m(\phi_i(\mathbf{x}_j^{\mathrm{gq}}))$ at each quadrature node.

3.1. Generalization to multiple subdomains

In the previous sections we decided to limit ourselves to the case where the domain of the PDE is partitioned into two subdomains. This choice is motivated mainly by the fact that considering the generic case of multiple subdomains leads necessarily to complexity in the notation. We refer the reader to the already mentioned references [4, 11] for examples of how the functional spaces we considered in Section 2 could be adapted to the case of multiple subdomains. One aspect that differentiates our approach from other methods (such as the mortar method) is that, in the discretization process, our method requires to define a set of basis functions for the Lagrange multiplier space of each interface. These bases can be chosen independently one from the other. In particular, in our numerical results we were able to recover optimal convergence without imposing any requirement on the values of the basis functions in the cross points.

As an example, Figure 1 (*left*) shows a three-way partition of Ω into three domains with three interfaces. Each of the interfaces Γ_1 and Γ_2 requires the definition of a corresponding space for the Lagrange multipliers. After the discretization, the matrix of the algebraic system can be written as displayed in Figure 1 (*right*), where the matrices $(B_{ij})_{mn} = \int_{\Gamma_i} \varphi_n^{(j)} \xi_m^{(i)} \, \mathrm{d}\mathbf{s}$ discretize the coupling between the jth domain and the ith interface. We remark that the signs of the coupling matrices are determined by the definition of the normals at each interface. Notice that, besides the choice of the orientation of the normals at the interfaces, there is no hierarchy among the subdomains.

In Section 6.3, we consider numerical results obtained on a domain whose partition is topologically equivalent to that presented in Figure 1.

4. Relationship with other non-conforming methods

4.1. Relationship with the mortar method

The mortar method can be derived from the same problem written in primal hybrid formulation W2 we considered in Section 2 [47]. Its discretized weak formulation could be rewritten in the form of a saddle-point problem similar to equation (2.7) in which the space of Lagrange multiplier Λ_M^h depends on the discretization of either Ω_1 or Ω_2; see [43, 44]. In particular, the classic mortar method requires assigning to Ω_1 or to Ω_2 the role

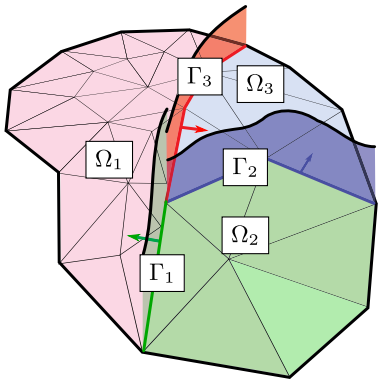

$$\begin{bmatrix} A_1 & 0 & 0 & B_{11}^T & 0 & B_{31}^T \\ 0 & A_2 & 0 & -B_{12}^T & -B_{22}^T & 0 \\ 0 & 0 & A_3 & 0 & B_{23}^T & -B_{33}^T \\ B_{11} & -B_{12} & 0 & 0 & 0 & 0 \\ 0 & -B_{22} & B_{23} & 0 & 0 & 0 \\ B_{31} & 0 & -B_{33} & 0 & 0 & 0 \end{bmatrix}$$

FIGURE 1. *Left panel*: example of a three-way partition of Ω with three interfaces; each interface corresponds to a Lagrange multiplier space. *Right panel*: corresponding system matrix obtained from the discretization of the spaces.

of master and slave domains. The basis functions of Λ_M^h are chosen as the trace of the basis functions defined over the triangulation of the slave domain which do not vanish on Γ; the polynomial order of the basis functions is usually decreased by one over the first and last elements of the partition of Γ.

With respect to the mortar method, we believe that the main advantages of our approach are the following:

(1) the accuracy of the coupling can be increased or decreased by varying the number of basis functions for the space Λ^δ independently of the discretization in the subdomains;
(2) the solution is independent of any classification of the subdomains into master and slaves, which is not required by the method;
(3) the computation of the coupling matrices does not require projections between meshes, which makes the implementation of the method easier.

One drawback of our method is that the Lagrange multiplier space has to be rich enough to provide the necessary accuracy, but coarse enough to satisfy the inf-sup condition as described in Section 5.

4.2. Relationship with INTERNODES

The INTERNODES (INTERpolation for NOnconforming DEcompositionS) method [25] is based on an interpolation approach, rather than the L^2-projection approach which characterizes the mortar method. Given each interface, the two adjacent subdomains are given the role of master and slave domains. Similarly to the mortar method, the traces of the (finite element or spectral element) basis functions defined over the meshes of the master and slave domains are used to enforce the continuity of the solution and the normal stresses. More precisely, two interpolation operators – or intergrid operators – are defined: the interpolation operator from the master to the slave domain is used to ensure the continuity of the solution, while the interpolation operator from the slave to the master domain enforces the continuity of the normal fluxes. INTERNODES has been proven to retain the optimal convergence properties of the mortar method.

Being INTERNODES closely related to the mortar method, compared to the former our approach offers the same advantages we presented in Section 4.1 except for 3. Indeed, INTERNODES has the big advantage of being simple to implement and allowing for non-matching interfaces, namely interfaces which could either feature (small) overlaps or holes between them; we refer to this situation as geometric non-conformity. We believe that our method is as simple to implement as INTERNODES and that it can be extended to non-conforming geometries with the help of localized Rescaled Radial Basis Interpolation [24, 27].

4.3. Relationship with the three-field method

The three-field method was originally proposed in [15] and analyzed in [14]. Compared to the mortar method, it has had significantly less impact on the domain decomposition community.

The multidomain extension of the weak formulation W1 by the three-field method reads [38]:

(W4) *for* $i = 1, 2$, *find* $u^{(i)} \in \mathcal{X}^{(i)}$, $\sigma^{(i)} \in H^{-1/2}(\Gamma)$ *and* $\psi \in H^{1/2}(\Gamma)$ *such that*

$$\begin{aligned}
&a(u^{(1)}, v^{(1)}) - \langle \sigma^{(1)}, v^{(1)} \rangle_{H^{-1/2}(\Gamma)} = \langle f, v^{(1)} \rangle && \forall v^{(1)} \in \mathcal{X}^{(1)},\\
&\langle \eta^{(1)}, \psi - u^{(1)} \rangle_{H^{-1/2}(\Gamma)} = 0 && \forall \eta^{(1)} \in H^{-1/2}(\Gamma),\\
&\langle \sigma^{(1)} + \sigma^{(2)}, \rho \rangle_{H^{-1/2}(\Gamma)} = 0 && \forall \rho \in H^{1/2}(\Gamma),\\
&\langle \eta^{(2)}, \psi - u^{(2)} \rangle_{H^{-1/2}(\Gamma)} = 0 && \forall \eta^{(2)} \in H^{-1/2}(\Gamma),\\
&a(u^{(2)}, v^{(2)}) - \langle \sigma^{(2)}, v^{(2)} \rangle_{H^{-1/2}(\Gamma)} = \langle f, v^{(2)} \rangle && \forall v^{(2)} \in \mathcal{X}^{(2)}.
\end{aligned} \tag{4.1}$$

It can be proven (see [38], Prop. 1.7.1) that if u is the solution of W1 and $u^{(i)}$, $\sigma^{(i)}$, ψ are solutions of W4, then $u^{(i)} = u|_{\Omega_i}$, $\sigma^{(i)} = (\nabla_L u \cdot \mathbf{n}_i)_\Gamma$ (where $\nabla_L u \cdot \mathbf{n}_i$ indicates the conormal derivative of u with respect to the normal vector $\mathbf{n}_i$), and $\psi = u|_\Gamma$.

The weak formulation W2 we derived in Section 2 can be interpreted as a particular case of W4. Indeed, let us firstly restrict the space $H^{1/2}(\Gamma)$ to its embedded subset $H_{00}^{1/2}(\Gamma)$ and let us consider the particular case in which $\lambda = \sigma^{(1)} = -\sigma^{(2)} \in \Lambda = H_{00}^{-1/2}(\Gamma)$: then, the third equation in equation (4.1) is automatically satisfied for all choices of $\rho \in H_{00}^{1/2}(\Gamma)$. Moreover, subtracting the second and fourth equations evaluated at the same $\eta^{(1)} = \eta^{(2)} = \eta \in \Lambda$ yields

$$\langle \eta, \psi - u^{(1)} \rangle_\Lambda - \langle \eta, \psi - u^{(2)} \rangle_\Lambda = \langle \eta, u^{(2)} - u^{(1)} \rangle_\Lambda. \tag{4.2}$$

Obviously, this duality is well defined only if the trace of $u^{(2)} - u^{(1)}$ belongs to $H_{00}^{1/2}(\Gamma)$. We, therefore, set $u \in \mathcal{X}_{00}$ such that $u^{(1)} = u|_{\Omega_1}$ and $u^{(2)} = u|_{\Omega_2}$; equation (4.2) can be then rewritten as $b(u, \eta) = 0$ for all $\eta \in \Lambda$, *i.e.* the second equation in equation (2.7). The first equation in equation (2.7) is found by adding the first and last equations in (4.1) tested for all $v \in \mathcal{X}_{00}$ such that $v^{(1)} = v|_{\Omega_1}$, $v^{(2)} = v|_{\Omega_2}$; observe that also in this case it is necessary to restrict the search space for v to $\mathcal{X}_{00}$, in order to ensure the well-posedness of $b(v, \lambda) = \langle \lambda, v^{(2)} - v^{(1)} \rangle_\Lambda$.

Although W2 and W4 are equivalent, their discretizations are not. Indeed, in the three-field method, it is necessary to define the discretizations of the variational spaces of $\sigma^{(1)}$, $\sigma^{(2)}$ and ψ. In contrast, when discretizing W2, the third equation of W4 is not approximated but solved exactly and the second and fourth are merged into a single equation. As we have shown, setting $\sigma^{(1)} = -\sigma^{(2)}$ is efficient because it allows to automatically satisfy the third equation in equation (4.1), thus reducing the number of variables. Our approach limits to one the number of spaces to be discretized for each interface, thus allowing better control of the stability of the method.

5. Inf-sup condition of the discretized problem

Problems W2 and W3 are saddle-point problems [37]. As such, their well-posedness depends on the inf-sup condition [12], also known as Ladyschenskaja-Babuka-Brezzi condition, which sets the requirements for the uniqueness of the solution as well as the stability of the sequence of problems depending on the discretization parameters (*e.g.* the mesh size h or the number of basis functions on the interface n_Γ). We refer the reader to [12,13] for a comprehensive description of the inf-sup condition from the functional and algebraic point of view respectively. In this section, we specifically address the well-posedness of W3, and we limit ourselves to recall that if the space Λ is characterized as in (2.5), the continuous problem W2 has a unique solution [11].

Before stating the main stability result for W3, we recall that we characterize $a(\cdot,\cdot)$ and $b(\cdot,\cdot)$ as continuous if there exist $\kappa_a > 0$ and $\kappa_b > 0$ such that $a(\varphi,\psi) \leq \kappa_a \|\varphi\|_{\mathcal{X}} \|\psi\|_{\mathcal{X}}$ for every $\varphi,\psi \in \mathcal{X}$ and $b(\varphi,\xi) \leq \kappa_b \|\varphi\|_{\mathcal{X}} \|\xi\|_{\Lambda}$ for every $\varphi \in \mathcal{X}$, $\xi \in \Lambda$.

The following theorem prescribes the conditions for the well-posedness of W3.

Theorem 5.1 ([13], Thm. 3.2)**.** *Assume that $a(\cdot,\cdot)$ and $b(\cdot,\cdot)$ are continuous with constants $k_a > 0$ and $k_b > 0$, and that there exist $\alpha > 0$ and $\beta > 0$ such that $\mathcal{X}^h$, $\mathcal{V}^{h,\delta}$ and Λ^δ satisfy the conditions*

$$\begin{aligned} \inf_{v^h \in \mathcal{V}^{h,\delta}} \frac{a(v^h, v^h)}{\|v^h\|_{\mathcal{X}}^2} &\geq \alpha, \\ \inf_{\eta^\delta \in \Lambda^\delta} \sup_{v^h \in \mathcal{X}^h} \frac{b(v^h, \eta^\delta)}{\|v^h\|_{\mathcal{X}} \|\eta^\delta\|_{\Lambda}} &\geq \beta. \end{aligned} \tag{5.1}$$

Then W3 has a unique solution. Moreover, there exists a constant $C \geq 0$, depending only on κ_a, κ_b, α and β, such that

$$\|u - u^h\|_{\mathcal{X}} + \|\lambda - \lambda^\delta\|_{\Lambda} \leq C \left(\inf_{v^h \in \mathcal{X}^h} \|u - v^h\|_{\mathcal{X}} + \inf_{\eta^\delta \in \Lambda^\delta} \|\lambda - \eta^\delta\|_{\Lambda} \right), \tag{5.2}$$

where (u,λ) is the solution of W2.

5.1. Numerical computation of the inf-sup constant

The inf-sup condition (5.1) is satisfied whenever Λ^δ is sufficiently "small" compared to $\mathcal{X}^h$. In the applications in Section 6 we ensure that β exists by numerically computing an approximation $\widetilde{\beta}$ with the approach presented in [2], which we briefly summarize here. Let us suppose that $X_{\mathcal{X}} \in \mathbb{R}^{(n_{\mathrm{bf}}^{(1)}+n_{\mathrm{bf}}^{(2)})\times(n_{\mathrm{bf}}^{(1)}+n_{\mathrm{bf}}^{(2)})}$ and $X_\Lambda \in \mathbb{R}^{n_\Gamma \times n_\Gamma}$ are norm matrices such that $\|v^h\|_{\mathcal{X}}^2 = (X_{\mathcal{X}}\mathbf{v},\mathbf{v})$ and $\|\eta^\delta\|_\Lambda^2 = (X_\Lambda \boldsymbol{\eta},\boldsymbol{\eta})$ for every $v \in \mathcal{X}^h$ and every $\eta \in \Lambda^\delta$. In the previous expressions, we denoted $(\cdot,\cdot)$ the standard scalar product in $\mathbb{R}^m$ ($m = n_{\mathrm{bf}}^{(1)} + n_{\mathrm{bf}}^{(2)}$ or $m = n_\Gamma$) and $\mathbf{v}$ and $\boldsymbol{\eta}$ the vectors of degrees of freedom of v^h and η^δ. Then, we have

$$\begin{aligned} \widetilde{\beta} &= \inf_{\eta^\delta \in \Lambda^\delta} \sup_{v^h \in \mathcal{X}^h} \frac{b(v^h,\eta^\delta)}{\|v^h\|_{\mathcal{X}} \|\eta^\delta\|_\Lambda} = \inf_{\boldsymbol{\eta}\neq\mathbf{0}} \sup_{\mathbf{v}\neq\mathbf{0}} \frac{(B\mathbf{v},\boldsymbol{\eta})}{(X_{\mathcal{X}}\mathbf{v},\mathbf{v})^{1/2}(X_\Lambda\boldsymbol{\eta},\boldsymbol{\eta})^{1/2}} \\ &= \inf_{\boldsymbol{\eta}\neq\mathbf{0}} \frac{1}{(X_\Lambda\boldsymbol{\eta},\boldsymbol{\eta})^{1/2}} \sup_{\substack{\mathbf{w}=X_{\mathcal{X}}^{1/2}\mathbf{v}\neq\mathbf{0} \\ \|\mathbf{w}\|=1}} \left(\mathbf{w}, X_{\mathcal{X}}^{-1/2} B^T \boldsymbol{\eta}\right) \\ &= \inf_{\boldsymbol{\eta}\neq\mathbf{0}} \frac{\left(X_{\mathcal{X}}^{-1/2}B^T\boldsymbol{\eta}, X_{\mathcal{X}}^{-1/2}B^T\boldsymbol{\eta}\right)^{1/2}}{(X_\Lambda\boldsymbol{\eta},\boldsymbol{\eta})^{1/2}} = \inf_{\boldsymbol{\eta}\neq\mathbf{0}} \frac{\left(BX_{\mathcal{X}}^{-1}B^T\boldsymbol{\eta},\boldsymbol{\eta}\right)^{1/2}}{(X_\Lambda\boldsymbol{\eta},\boldsymbol{\eta})^{1/2}}. \end{aligned}$$

We remark that the equivalence between the second and the third line of the last equation comes from the fact that the unitary vector $\mathbf{w}$ maximizing its scalar product with $\mathbf{y} = X_{\mathcal{X}}^{-1/2}B^T\boldsymbol{\eta}$ is $\mathbf{w} = \mathbf{y}/(\mathbf{y},\mathbf{y})^{1/2}$ by the Cauchy–Schwarz inequality. Introducing now the following generalized eigenvalue problem

$$\begin{bmatrix} X_{\mathcal{X}} & B^T \\ B & 0 \end{bmatrix} \begin{bmatrix} \mathbf{v} \\ \boldsymbol{\eta} \end{bmatrix} = -\sigma \begin{bmatrix} 0 & 0 \\ 0 & X_\Lambda \end{bmatrix} \begin{bmatrix} \mathbf{v} \\ \boldsymbol{\eta} \end{bmatrix}, \tag{5.3}$$

and recognizing that we have

$$BX_{\mathcal{X}}^{-1}B^T\boldsymbol{\eta} = \sigma X_\Lambda \boldsymbol{\eta} \quad \Rightarrow \quad \sigma = \frac{\left(BX_{\mathcal{X}}^{-1}B^T\boldsymbol{\eta},\boldsymbol{\eta}\right)}{(X_\Lambda\boldsymbol{\eta},\boldsymbol{\eta})}, \tag{5.4}$$

we conclude that $\widetilde{\beta}$ can be computed as the square root of the minimum eigenvalue of equation (5.3), *i.e.* $\widetilde{\beta} = \sqrt{\sigma_{\min}}$. For an application of this strategy, we refer the reader to the results presented in Figure 5.

5.2. Convergence result for saddle-point problems

We close this section by focusing on the convergence of problem W3. The following proposition gives a sharper bound than equation (5.2) to the estimate of the approximation error. The proof can be found *e.g.* in Theorem 16.6 from [37] or in the derivation of equation (5.2) in [28].

Proposition 5.2. *Let the assumptions of Theorem 5.1 be satisfied. Then the solution* (u, λ) *of W2 and the solution* (u^h, λ^δ) *of W3 satisfy the following error estimates*

$$\|u - u^h\|_{\mathcal{X}} \leq \left(1 + \frac{\kappa_a}{\alpha}\right) \inf_{v_*^h \in \mathcal{V}^{h,\delta}} \|u - v_*^h\|_{\mathcal{X}} + \frac{\kappa_b}{\alpha} \inf_{\eta^\delta \in \Lambda^\delta} \|\lambda - \eta^\delta\|_\Lambda, \tag{5.5}$$

$$\|\lambda - \lambda^\delta\|_\Lambda \leq \frac{\kappa_a}{\beta}\left(1 + \frac{\kappa_a}{\alpha}\right) \inf_{v_*^h \in \mathcal{V}^{h,\delta}} \|u - v_*^h\|_{\mathcal{X}} + \left(1 + \frac{\kappa_b}{\beta} + \frac{\kappa_a \kappa_b}{\alpha\beta}\right) \inf_{\eta^\delta \in \Lambda^\delta} \|\lambda - \eta^\delta\|_\Lambda. \tag{5.6}$$

Moreover, the following error estimate holds

$$\inf_{v_*^h \in \mathcal{V}^{h,\delta}} \|u - v_*^h\|_{\mathcal{X}} \leq \left(1 + \frac{\kappa_b}{\beta}\right) \inf_{v^h \in \mathcal{X}^h} \|u - v^h\|_{\mathcal{X}}. \tag{5.7}$$

Proposition 5.2 shows that, whenever the space of Lagrange multipliers is rich enough (namely the second term in equation (5.5) becomes negligible compared the first one), the approximation of u is essentially bounded by the best approximation error on $\mathcal{X}$. However, this richness may lower the inf-sup constant β and therefore loose the approximation (5.7). It is therefore important to find the correct balance.

We remark that from equation (3.1) we have that increasing the size of the Lagrange multipliers space is equivalent to lowering the size of $\mathcal{V}^{h,\delta}$ and, consequently, the supremum in its right hand side. The two error estimates in (3.1) and (5.5) are therefore equivalent ways of expressing the fact that, if the continuity over the interface Γ is enforced strongly enough, the error converges to zero as the error due to the spatial discretization in $\mathcal{X}^h$. As we show in the next section, we are then able to recover the usual convergence orders for u with respect to the mesh size h when using FEM.

6. Numerical results

In this section, we focus on the performance of the method presented in Section 2 on two dimensional and three dimensional problems. The numerical simulations in two dimensions are performed with a set of Matlab scripts which can be freely downloaded[2]. The results we discuss in Section 6.3.2 are obtained with GeoPDEs [46], a free and open source package written in Octave and Matlab for IGA. The three dimensional results in Section 6.2.2 has been obtained using LifeV [8], a C++ library for high performance numerical simulations with FEM.

For all the simulations, we employ standard piecewise polynomial Lagrangian basis functions defined over suitable triangulations in the subdomains or B-Splines basis functions, as presented in Section 6.3.2. Regarding the choice of basis functions for Λ^δ, we already anticipated in Section 2 that in this paper we investigate the possibility of using low-frequency Fourier basis functions built on the interface Γ.

Remark 6.1. All the linear systems arising in the numerical simulations, except those in Section 6.2.2, are solved by means of the backslash operator in Matlab without any preconditioning.

[2] https://github.com/lucapegolotti/coupling_scripts

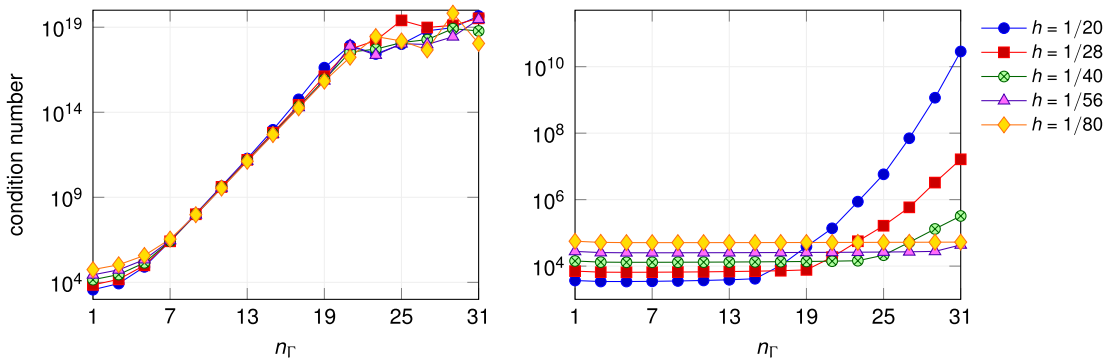

FIGURE 2. Condition number of the discretized system for the Poisson problem on two subdomains (see Sect. 6.2) *vs.* number of basis functions for the Lagrange multiplier space n_Γ. On the left, we consider the non-orthonormal basis functions in equation (6.1), while on the right we consider their orthonormalization.

6.1. Choice of basis functions for the Lagrange multipliers

In this section, we focus on the discretization of one dimensional interfaces. We will provide an example of how our approach can be generalized to two dimensional surfaces in Section 6.2.2.

Given an interface with length L, we consider $\xi_1 = 1$ and, for $i = 1, \dots, n_\omega$

$$\xi_{2i}(s) = \sin(\omega_i \pi s), \quad \xi_{2i+1}(s) = \cos(\omega_i \pi s), \tag{6.1}$$

where s is the arc length of the interface Γ, $\omega_i = i/L$, and n_ω is the number of considered frequencies; it holds that $n_\Gamma = 2n_\omega + 1$. With this definition, the set $\{\xi_i\}_{i=1}^{n_\Gamma}$ forms an orthogonal basis with respect to the $L^2(0, 2L)$ scalar product. We choose to employ such basis – instead of the standard Fourier basis orthogonal (or orthonormal) with respect to the $L^2(0, L)$ scalar product – because, by considering basis functions with periodicity L, we would impose an unnecessary periodicity constraint, in particular, the equality of the functions in Λ^δ and their derivatives at the extrema of Γ. As a result, we empirically observed that by employing the standard $L^2(0, L)$ orthonormal Fourier basis functions the optimal convergence of FEM is retrieved for larger values of n_Γ compared to the choice in equation (6.1). However, employing non-orthonormal basis functions (6.1) has a dramatic influence on the condition number of the resulting linear system, which has exponential growth with the increasing number of basis functions on the interface; see Figure 2 (*left*).

In order to retain the convergence order attained by using the Fourier modes in equation (6.1) and, at the same time, control the condition number of the system, we propose an orthonormalization strategy based on the Gram-Schmidt algorithm or, equivalently, on the QR decomposition [41]. Even though the coefficients of the orthonormal basis generated by (6.1) with these algorithms could be analytically derived, their exact expression quickly becomes complex with n_Γ becoming large. With our approach, we aim at obtaining an approximation of such coefficients relying on a fine sampling of the basis functions on the interval $(0, L)$. We remark that, in addition to allowing to effortlessly compute a large number of orthonormal basis functions, our approach has the advantage to be general enough to be applied to any set of non-orthonormal basis functions.

Let $\{\xi_i\}_{i=1}^{n_\Gamma}$ be the set of non-orthonormal basis functions defined on Γ. Moreover, let $\{x_i\}_{i=1}^{n_s}$ be distinct sample points distributed over the interval $(0, L)$, where L still denotes the length of the interface. We now introduce the functions $\{\kappa_i\}_{i=1}^{n_s}$, which we identify with the set of standard Lagrangian piecewise linear basis functions centered on each sample point x_i, and the associated mass matrix $M_{ij} = \int_\Gamma \kappa_i \kappa_j \, \mathrm{d}\mathbf{x}$. Furthermore, let $V = [\mathbf{v}_1, \mathbf{v}_2, \dots, \mathbf{v}_{n_\Gamma}] \in \mathbb{R}^{n_s \times n_\Gamma}$ be the matrix of the evaluations of the basis functions on the sample points, namely $V_{ij} = \xi_j(x_i)$. We remark that, for each $i = 1, 2, \dots, n_\Gamma$, we have $\|\xi_i\|^2_{L^2(0,L)} \approx \mathbf{v}_i^T M \mathbf{v}_i$. Since M is a positive-definite matrix, it admits a unique Cholesky decomposition and there exists $C \in \mathbb{R}^{n_s \times n_s}$ such that

$C^TC = M$. Let us now consider the unit matrix $Q \in \mathbb{R}^{n_s \times n_\Gamma}$ and the upper triangular matrix $R \in \mathbb{R}^{n_\Gamma \times n_\Gamma}$ such that the truncated QR decomposition of CV reads

$$CV = QR.$$

By construction, we have

$$(C^{-1}Q)^T M C^{-1}Q = Q^T C^{-T} C^T C C^{-1} Q = I,$$

thus, the columns of $C^{-1}Q$ represent evaluations at the sample points of functions orthonormal on $(0, L)$ with respect to the L^2 product. The matrix R performs the change of variable from the frame of reference of the new orthonormal basis functions to the frame of reference of the non-orthonormal basis functions. If the sampling is sufficiently fine, we speculate that the elements of the matrix R^{-1} well approximate the coefficients which are computed by applying the Gram-Schmidt algorithm to the continuous non-orthonormal basis functions $\{\xi_i\}_{i=1}^{n_\Gamma}$ and, in particular, that

$$\xi_i^{\mathrm{GS}} = \sum_{j=1}^{n_\Gamma} \xi_j R_{ji}^{-1}. \tag{6.2}$$

From a practical perspective, the matrix R^{-1} is suitable to compute the coupling matrix B^{GS} with respect to the orthonormal Fourier basis functions, knowing the coupling matrix computed without orthonormalization B. Indeed, we have

$$B_{ij}^{\mathrm{GS}} = \int_\Gamma \xi_i^{\mathrm{GS}} \varphi_j \, \mathrm{d}\mathbf{s} = \sum_{k=1}^{n_\Gamma} \left(\int_\Gamma \xi_k \varphi_j \, \mathrm{d}\mathbf{s} \right) R_{ki}^{-1} = \sum_{k=1}^{n_\Gamma} B_{kj} R_{ki}^{-1},$$

or equivalently $B_{ij}^{\mathrm{GS}} = R^{-T} B$. Observe that, being R an upper triangular matrix, the application of R^{-T} is performed at negligible cost and that the matrix R^{-T} depends only on the choice of the non-orthonormal basis functions and can be then computed *a priori*. We remark that, with this approach, the orthonormal basis functions are never explicitly computed. Moreover, since the discrete space is exactly the same, the approximation properties and the convergence orders are not changed. Figure 2 (*right*) shows that, after the orthonormalization of the Fourier basis functions (6.1) by the algorithm we presented, the system is more stable and the condition number increases with the number of Fourier basis functions n_Γ dependently on the refinement level of the mesh h.

6.2. The Poisson problem on two-way partitioned domains

6.2.1. Results in two dimensions on the unit square

Let us consider the global Poisson problem (2.2) on the domain $\Omega = (0,1)^2$, where we take f such that $u = 100xy(1-x)(1-y)\sin(1/3 - xy^2)$ is the exact solution. We divide Ω into $\Omega_1 = (0, 0.5) \times (0, 1)$ and $\Omega_2 = (0.5, 1) \times (0, 1)$.

We numerically solve the problem on Ω_1 and Ω_2 by employing structured triangular conforming and non-conforming meshes with varying mesh size h. The conforming meshes are obtained by subdividing the domain in the x- and y-direction in the same number of elements. On the other hand, the non-conforming meshes are built by taking in the y-direction of Ω_2 $N+1$ elements, N being the number of elements in the y-direction in Ω_1 as well as the total number of elements in the x-direction.

Figure 3 shows how the solutions on Ω_1 and Ω_2 obtained with a conforming mesh with $N = 20$ elements in each direction change with respect to the number of basis functions on the interface. The results are obtained with quadratic Lagrangian polynomials in both subdomains. From the contour lines plots in the top row, it appears that the two solutions match quite accurately at the interface with 5 Fourier basis functions ($n_\omega = 2$). In the second row of Figure 3, we plot the approximation by finite differences of the derivative of the solution with respect to x in the two domains, which is equal to the normal derivative of $u^{h,(1)}$ and to the opposite of the normal derivative on $u^{h,(2)}$ on Γ respectively. Observe that, as we already highlighted in Remark 2.4, the Lagrange multiplier λ^δ takes the role of the normal derivative of u^h on Γ.

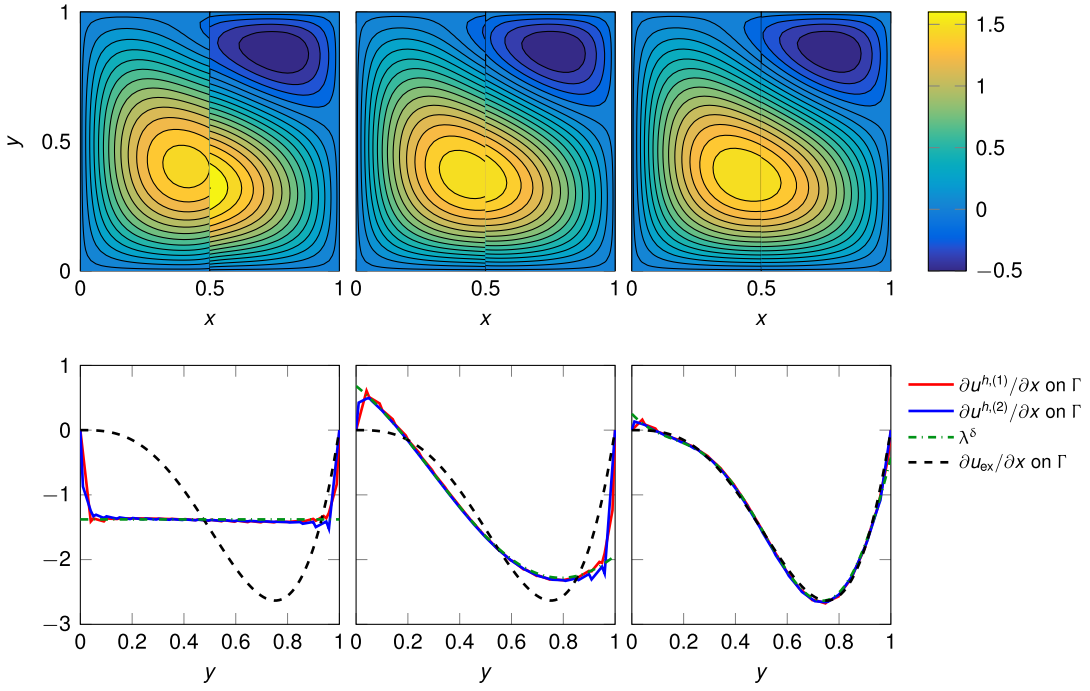

FIGURE 3. Contour lines of the solution (*top row*) and derivatives of the solution at both sides of the interface, approximated Lagrange multiplier and exact derivative at the interface (*bottom row*) when $n_\Gamma = 1$ (*left column*), $n_\Gamma = 3$ Fourier modes (*middle column*) and $n_\Gamma = 5$ Fourier modes (*right column*) are used to characterize the space Λ^δ.

Let us now address the convergence of the global solution to the exact one with respect both to the mesh size h and the number of basis functions on the interface n_Γ. To this end, we consider meshes with total number of elements in the x-direction $N = 20, 28, 40, 56, 80, 114, 160$ and we solve the problems by employing quadratic Lagrangian basis functions in both subdomains. Figure 4 (*top row*) depicts the decaying of the error in $\mathcal{X}$-norm (the broken norm) with respect to h, as well as the convergence of the error obtained by solving the problem on a single conforming mesh of Ω (in black dashed line). When employing both conforming and non-conforming meshes, the error is optimal – in the sense that we recover the theoretical order of convergence h^2 of quadratic finite elements for the H^1-error – when n_Γ is large enough, *e.g.* $n_\Gamma \geq 13$. In this case, the error is equal to the one given by the single domain approach. If n_Γ is too small, on the contrary, the solution is unable to converge to the exact solution with h and reaches a stagnation point. We remark that this result is perfectly consistent with Strang's second lemma (3.1) and with the stability result in Proposition 5.2: whenever the space of Lagrange multiplier is rich enough (which is equivalent to requiring that $\mathcal{V}^{h,\delta}$ be a good approximation of $\mathcal{V}$), the best approximation error of the interpolation is recovered.

Remark 6.2. In our numerical simulations with non-conforming meshes, we observed that instabilities arise when using coarse meshes and low-order quadrature rules for the computations of the approximate integrals of B_1 and B_2 in equation (3.4). When considering, for example, $h = 1/20, 1/28, 1/40$ and 2 Gauss quadrature nodes, the error starts increasing when n_Γ becomes large (*e.g.* $n_\Gamma \geq 15$). By increasing the order of the quadrature rule and choosing 4 Gauss quadrature nodes this issue is completely fixed. We did not encounter stability problems when using conforming meshes, even with low-order quadrature rules.

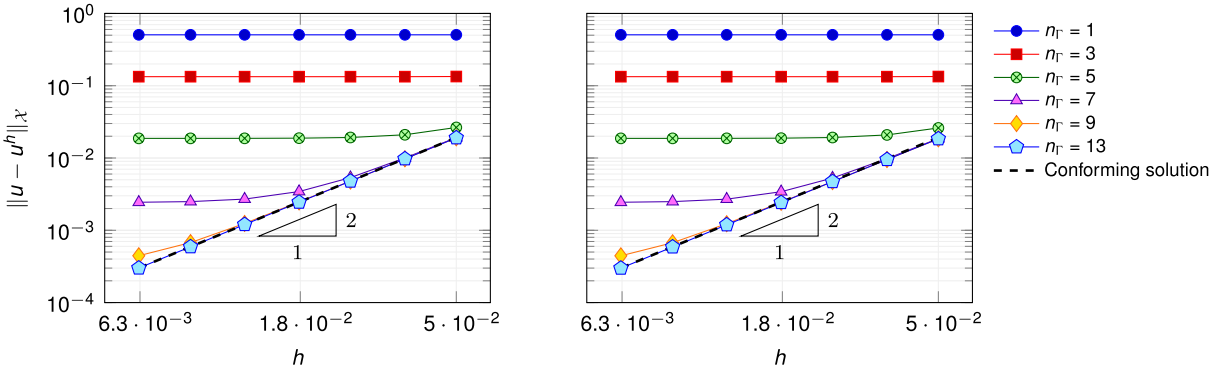

FIGURE 4. Convergence of error in broken norm with respect to the mesh size h and number of basis functions on the interface n_Γ with conforming (*left panel*) and non-conforming meshes (*right panel*).

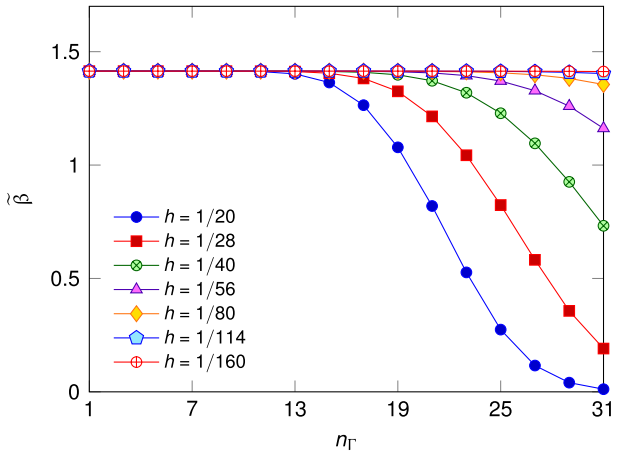

FIGURE 5. Decaying of the inf-sup constant $\widetilde{\beta}$ with respect to n_Γ.

Figure 5 shows the variation of the estimate of the inf-sup constant $\widetilde{\beta}$ – computed as the square root of the minimum eigenvalue of the generalized eigenvalue problem (5.3), as described in Section 5.2 – when the number of basis functions on the interface changes; the estimate refers to the simulation of the Poisson equations with conforming meshes and quadratic polynomial basis functions. Due to the difficulties in computing the $H_{00}^{-1/2}$-norm for the Lagrange multiplier, we replaced the estimate given by equation (5.3) with a surrogate where the space $\mathcal{X}^h$ is substituted with the space spanned by the traces on Γ of the finite element basis functions φ_i; the L^2-norm is used both for such space – we denote $\mathcal{X}_{L^2(\Omega)}$ the corresponding mass matrix – and Λ^δ. For the result in Figure 5, we employed the orthonormal basis functions ξ_i^{GS} computed as in equation (6.2), so that $X_\Lambda = I$; therefore, from equation (5.4) it follows that $\widetilde{\beta}$ is simply found as the square root of the minimum eigenvalue of $B^{\mathrm{GS}}\mathcal{X}^{-1}_{L^2(\Omega)}(B^{\mathrm{GS}})^T$. In Figure 5, each curve presents a plateau phase in which the inf-sup constant stays approximately constant at around $\widetilde{\beta} \approx 1.41$ with the increment of n_Γ. The width of such plateau phase increases when h becomes smaller. Indeed, we observe that $\widetilde{\beta}$ starts decreasing for smaller values of n_Γ when the meshes are coarser and that, conversely, for finer meshes the inf-sup constant varies relatively little in the range $n_\Gamma \in (1, 31)$. We remark that, combined with the condition number shown in Figure 2 (*right*), this result

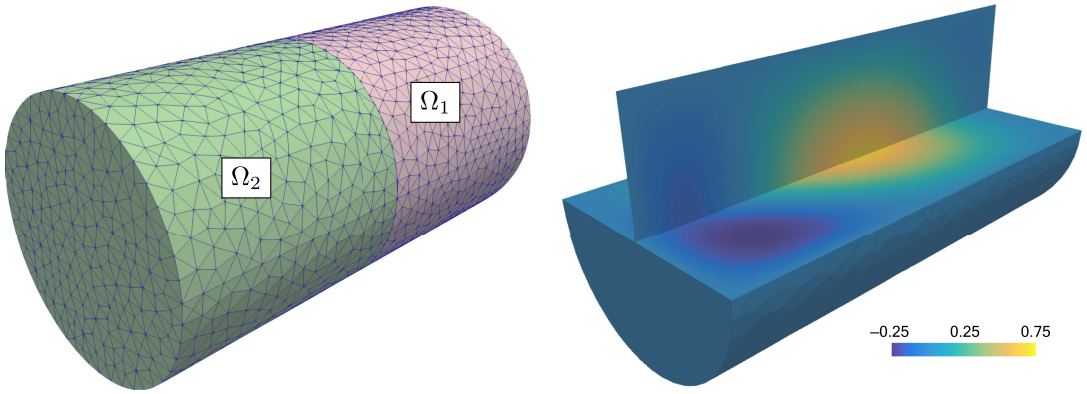

FIGURE 6. *Left panel*: subdomains of the cylinder with corresponding meshes (sizes: $h_1 = 1.61 \cdot 10^{-1}$ and $h_2 = 1.76 \cdot 10^{-1}$). *Right panel*: the solution u obtained with $n_\Gamma = 28$.

ensures that for each refinement level, we are able to obtain the optimal convergence of FEM when the basis functions are orthonormal. Indeed, refining the mesh has the effect of both increasing the range of stability of the linear system – see Figure 2 (*right*) – and increasing the number of basis functions on the interface that can be employed without reaching the fast decaying region of $\widetilde{\beta}$ in Figure 5. With regard to this last point, we recall that it is important to prevent the inf-sup constant to become too small because it appears at the denominator of the constant multiplying the best approximation errors on u and on λ in the error estimates of Proposition 5.2.

6.2.2. Results in three dimensions on a cylinder

We consider the Poisson problem (2.2) on a three dimensional domain. In particular, we take the cylinder

$$\Omega = \{\mathbf{x} = [x, y, z]^T \in \mathbb{R}^3 : x \in (0, 2),\ y^2 + z^2 < R^2\},$$

where $R = 1/2$, and we set the forcing term f such that

$$u = 25 \left(\frac{x}{2} - \frac{\exp(x) - 1}{\exp 2 - 1} \right) (R^2 - y^2 - z^2) \sin(x - y) \sin(x - z)$$

is the exact solution.

We consider the subdomains Ω_1 and Ω_2 obtained by cutting the domain with the plane corresponding to $x = 1$. On each subdomain, we define a family of triangulations $\mathcal{T}^{(1)}$ and $\mathcal{T}^{(2)}$ composed of tetrahedra such that, for each couple $(\mathcal{T}^{h,(1)}, \mathcal{T}^{h,(2)}) \in \mathcal{T}^{(1)} \times \mathcal{T}^{(2)}$, the resulting mesh is not conforming at the interface. Figure 6 (*left*) displays one of such global triangulations of the computational domain. We consider finite element spaces composed of standard Lagrangian linear and quadratic basis functions on Ω_1 and Ω_2 respectively.

For what concerns the discretization of the Lagrange multipliers space, in this test case we exploit the fact that the interface Γ is a circle (before the geometric discretization of Ω). We define on the plane $x = 1$ a polar system of coordinates centered in $\mathbf{x}_0 = (1, 0, 0)$ and we denote by $u = \sqrt{y^2 + z^2}$ and $v = \theta(y, z)$ the two parametric variables representing the radial distance from the point $\mathbf{x}_0$ and the angular variable. The function $\theta(\cdot, \cdot)$ is defined as $\theta(y, z) = \arctan(z/y)$ if $y \geq 0$ and $\theta(y, z) = \arctan(z/y) + \pi$ if $y < 0$. We define in each of the parametric directions a set of basis functions. In the radial direction, we take $\xi^u_{i+1}(u) = \cos(\pi i u/4R)$, for $i = 0, \ldots, n^u_\omega$; we employ only cosines with varying frequencies in order to avoid discontinuities in the derivatives at $u = 0$. In the angular direction, we take $\xi^v_1(v) = 1$, $\xi^v_{2i}(v) = \sin(i\pi v)$ and $\xi^v_{2i+1}(v) = \cos(i\pi v)$, with $i = 1, \ldots, n^v_\omega$. The two dimensional basis functions on the interface are then defined by means of the tensor

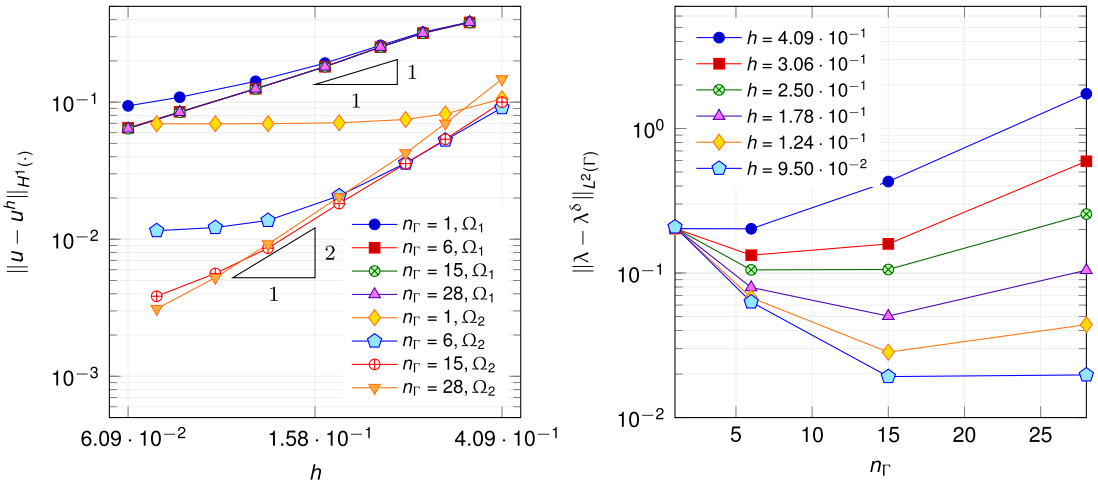

FIGURE 7. Convergence of the H^1-error on the solution u in Ω_1 and Ω_2 (*left panel*) and convergence of the L^2-error on the Lagrange multiplier λ (*right panel*).

product of these two sets of univariate basis functions, namely we define $\xi_{ij}(u,v) = \xi_i^u(u)\xi_j^v(v)$ and the total number of such basis functions is $n_\Gamma = (n_\omega^u + 1)(2n_\omega^v + 1)$. In our tests, we consider to simplify the analysis of the results $n_\omega^u = n_\omega^v$, but the resolution in the two parametric directions is *a priori* independent.

Figure 7 shows, on the left, the convergence of the H^1-error of u in Ω_1 and Ω_2 and, on the right, the convergence of the L^2-error on the Lagrange multiplier λ. The error on the solution converges (if n_Γ is high enough, consistently with what observed in Sect. 6.2.1) in each subdomain with the theoretical rate of the employed finite element space: order one in Ω_1, where linear finite elements are used, and order two in Ω_2, which has been discretized by using quadratic finite elements. If, on the other hand, the Lagrange multiplier space is not sufficiently rich, the error does not converge when h goes to zero. We remark that, being the error in Ω_1 larger than that in Ω_2 by one order of magnitude, the theoretical convergence of order one is achieved for smaller n_Γ in that subdomain. The L^2-error on the Lagrange multiplier, however, is not monotonic with respect to the number of basis functions n_Γ; see Figure 7 (*right*). In particular, for larger mesh sizes the error rapidly increases with n_Γ, whereas for smaller mesh sizes the error reaches a minimum for n_Γ strictly smaller than $n_\Gamma = 28$. This effect is clearly related to the inf-sup stability of the problem and to the fact that, as we already noticed in Section 6.2.1, the inf-sup constant β rapidly goes to zero with n_Γ if the mesh size is too large. The effect of the inf-sup condition being violated is also visible in the plot on the left, where for coarse meshes the error in Ω_2 increases with the addition of basis functions for Λ^δ; however, the increase in the error on the solution is not as evident as that on the Lagrange multiplier. One plausible explanation for the inf-sup stability of the problem having a larger impact on the accuracy of λ than the accuracy of u is that, by combining equations (5.6) and (5.7), we see that β^2 appears at the denominator in the error estimate of the Lagrange multiplier, whereas the constants in the error estimate for u in equation (5.5) depend on $1/\beta$.

For this test case we solve the linear system by the GMRES method with tolerance 10^{-8}. We also employ the block diagonal preconditioner

$$P = \begin{bmatrix} A_1 & 0 & 0 \\ 0 & A_2 & 0 \\ 0 & 0 & M \end{bmatrix},$$

where A_1 and A_2 are the stiffness matrices in the two subdomains and $M_{ij} = (\xi_j, \xi_i)_\Gamma$ is the mass matrix of Λ^δ, which is computed by selecting the finest mesh on the interface Γ for the numerical integration. During the application of the preconditioner, each diagonal block is solved by an LU decomposition. Figure 8 shows

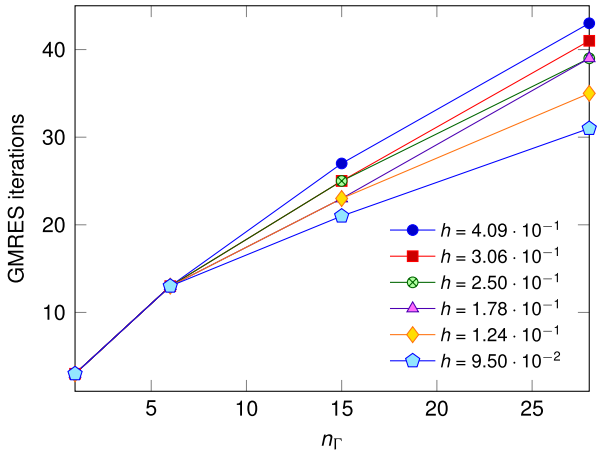

FIGURE 8. GMRES iterations for solving the (preconditioned) linear system on the problem presented in Section 6.2.2 *vs.* number of basis functions for the Lagrange multiplier space.

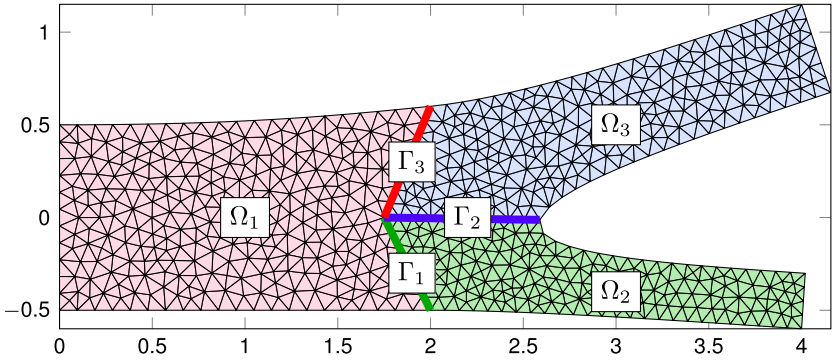

FIGURE 9. Three-way partition of the model bifurcation. The displayed mesh corresponds to the size $h = 1.32 \cdot 10^{-1}$.

how the the number of GMRES iterations varies with respect to n_Γ and the mesh size. Clearly, the number of iterations increases by enriching the basis functions on the interface. Nevertheless, it also appears that the number of iterations decreases when the mesh size becomes smaller. This is a consequence of the fact that, for a fixed n_Γ, the conditioning and the inf-sup stability of the coupling improve when h becomes smaller (as shown in Figs. 2 and 5).

6.3. The Navier–Stokes steady equations on three-way partitioned domains

In this section, we test the flexibility of our method by solving the steady Navier–Stokes equations in the domain $\Omega \in \mathbb{R}^2$ depicted in Figure 9, which represents an idealized bifurcation in an arterial tree. The equations read

$$\begin{aligned} -\mu\Delta\mathbf{u} + (\mathbf{u}\cdot\nabla)\mathbf{u} + \nabla p &= \mathbf{f} \quad \text{in } \Omega, \\ \operatorname{div}\mathbf{u} &= 0 \quad \text{in } \Omega, \end{aligned} \tag{6.3}$$

with $\mathbf{u} = \mathbf{g}$ on Γ_D and $\sigma(\mathbf{u}, p)\mathbf{n} = \mathbf{h}$ on Γ_N. Here, $\mathbf{u}$ and p are velocity and pressure respectively, $\mu \in \mathbb{R}^+$ is the viscosity, Γ_D and Γ_N are portions of the boundary such that $\Gamma_D \cap \Gamma_N = \partial\Omega$ and $\Gamma_D \cup \Gamma_N = \emptyset$, $\mathbf{f}$ is a given

forcing term, $\mathbf{g}$ and $\mathbf{h}$ are the Dirichlet and Neumann boundary data respectively, and

$$\sigma(\mathbf{u}, p) = \mu \nabla \mathbf{u} - pI$$

is the stress tensor. In all the test cases we consider, we take $\Gamma_D = \Gamma_{\text{in}} \cup \Gamma_{\text{w}}$, where $\Gamma_{\text{in}} = \{0\} \times (-r_{\text{in}}, r_{\text{in}})$ with $r_{\text{in}} = 0.5$ is the inflow boundary on the left and Γ_{w} is the wall of the vessel. The Neumann boundary $\Gamma_N = \Gamma_{\text{out}_1} \cup \Gamma_{\text{out}_2}$ is composed of the two outflows on the right. The Dirichlet boundary data is $\mathbf{g} = (y^2/r_{\text{in}}^2 - 1)U\mathbf{n}$ on Γ_{in} (where $\mathbf{n}$ is the outward normal to the inflow boundary), namely we impose a longitudinal parabolic inflow with maximum velocity magnitude U, and $\mathbf{g} = \mathbf{0}$ on Γ_{w} (no-slip condition). On the outflows Γ_N we set homogeneous Neumann conditions, *i.e.* $\mathbf{h} = \mathbf{0}$. In the numerical simulations, we set $\mu = 1$, $U = 1$ and $\mathbf{f} = \mathbf{0}$.

Let us briefly consider the spatial discretization of the Navier–Stokes equations in two dimensions. For a more complete treatment, the reader is referred to *e.g.* [37]. Let $\mathcal{V} = [H^1(\Omega)]^2$ be the space of functions with two components belonging to $H^1(\Omega)$ and let $\mathcal{Q} = L^2(\Omega)$ be the space of square integrable functions. For all $\boldsymbol{\varphi} \in \mathcal{V}$, $\boldsymbol{\psi} \in \mathcal{Q}$ we introduce the bilinear forms $a(\boldsymbol{\varphi}, \boldsymbol{\psi}) = (\mu \nabla \boldsymbol{\varphi}, \nabla \boldsymbol{\psi})_\Omega$ and $c(\boldsymbol{\varphi}, \boldsymbol{\psi}) = ((\boldsymbol{\varphi} \cdot \nabla)\boldsymbol{\varphi}, \boldsymbol{\psi})_\Omega$. Moreover, let $d(\boldsymbol{\varphi}, \phi) = -(\text{div}\boldsymbol{\varphi}, \phi)_\Omega$ for all $\boldsymbol{\varphi} \in \mathcal{V}$ and for all $\phi \in \mathcal{Q}$. The weak formulation of (6.3) reads

(W5) *given* $\mathbf{f} \in \mathcal{V}'$, $\mathbf{g} \in [H^{1/2}(\Gamma_N)]^2$, *and* $\mathbf{h} \in ([H^{1/2}(\Gamma_N)]^2)'$, *find* $(\mathbf{u}, p) \in \mathcal{V} \times \mathcal{Q}$, *such that*

$$\begin{aligned} a(\mathbf{u}, \mathbf{v}) + c(\mathbf{u}, \mathbf{v}) + d(\mathbf{v}, p) &= \langle \mathbf{f}, \mathbf{v} \rangle + \langle \mathbf{h}, \mathbf{v} \rangle_{\Gamma_N} \quad && \forall \mathbf{v} \in \mathcal{V}, \\ d(\mathbf{u}, q) &= 0 && \forall q \in \mathcal{Q} \end{aligned} \tag{6.4}$$

and such that $\mathbf{u}|_{\Gamma_D} = \mathbf{g}$.

Let us consider the finite dimensional approximations of the velocity $\mathbf{u}^h = \sum_{i=1}^{n_u} \boldsymbol{\varphi}_i u_i$ and the pressure $p^h = \sum_{i=1}^{n_p} \phi_i p_i$. Upon discretization of equation (6.4) by a Galerkin method – in this section, we consider FEM and IGA – the system can be rewritten in algebraic form as

$$\underbrace{\begin{bmatrix} A + C(\mathbf{w}) & D^T \\ D & 0 \end{bmatrix}}_{\mathcal{A}(\mathbf{w})} \mathbf{w} = \underbrace{\begin{bmatrix} \mathbf{r} \\ 0 \end{bmatrix}}_{\mathbf{F}}, \tag{6.5}$$

where $\mathbf{w} = [u_1, \dots, u_{n_u}, p_1, \dots, p_{n_p}] \in \mathbb{R}^{n_u + n_p}$ is a vector containing n_u degrees of freedom for the velocity and n_p degrees of freedom for the pressure, $A_{ij} = a(\boldsymbol{\varphi}_j, \boldsymbol{\varphi}_i)$, $[C(\mathbf{w})]_{ij} = ((\nabla \cdot \boldsymbol{\varphi}_j)\mathbf{u}^h, \boldsymbol{\varphi}_i)$ (where $\mathbf{u}^h$ is obtained by linear combination of the basis functions $\boldsymbol{\varphi}_k$ multiplied by the degrees of freedom of the velocity in $\mathbf{w}$), $D_{ij} = d(\boldsymbol{\varphi}_j, \phi_i)$ and $\mathbf{r}_i = (\mathbf{f}, \boldsymbol{\varphi}_i) + (\mathbf{h}, \boldsymbol{\varphi}_i)_{\Gamma_N}$.

Let us now introduce a partition of the domain Ω into three subdomains $\{\Omega_i\}_{i=1}^3$ separated by three interfaces $\{\Gamma_i\}_{i=1}^3$, as shown in Figure 9. Since the subdomains are topologically arranged as the ones presented in Section 3.1, the matrix of the global system maintains the structure of that presented in Figure 1. The global system reads

$$\begin{bmatrix} \mathcal{A}_1(\mathbf{w}_1) & 0 & 0 & B_{11}^T & 0 & B_{31}^T \\ 0 & \mathcal{A}_2(\mathbf{w}_2) & 0 & -B_{12}^T & -B_{22}^T & 0 \\ 0 & 0 & \mathcal{A}_3(\mathbf{w}_3) & 0 & B_{23}^T & -B_{33}^T \\ B_{11} & -B_{12} & 0 & 0 & 0 & 0 \\ 0 & -B_{22} & B_{23} & 0 & 0 & 0 \\ B_{31} & 0 & -B_{33} & 0 & 0 & 0 \end{bmatrix} \begin{bmatrix} \mathbf{w}_1 \\ \mathbf{w}_2 \\ \mathbf{w}_3 \\ \boldsymbol{\lambda}_1 \\ \boldsymbol{\lambda}_2 \\ \boldsymbol{\lambda}_3 \end{bmatrix} = \begin{bmatrix} \mathbf{F}_1 \\ \mathbf{F}_2 \\ \mathbf{F}_3 \\ \mathbf{0} \\ \mathbf{0} \\ \mathbf{0} \end{bmatrix}, \tag{6.6}$$

where $\mathcal{A}_i$ and $\mathbf{F}_i$ are the matrix and right hand side of system (6.5) referred to the ith subdomain, whereas B_{ij} is – as explained in Section 3.1 – the matrix discretizing the coupling of Ω_j and the interface Γ_i. For $i = 1, 2, 3$, the vector $\boldsymbol{\lambda}_i$ contains the Lagrange multipliers corresponding to the ith interface. Even in three dimensions, the computation of B_{ij} is straightforward and does not require projections or interpolations between meshes. Indeed, the value of the basis functions at each interface is known *a priori*.

Remark 6.3. When applied to the Navier–Stokes equations in two dimensions, the method requires assigning to each interface two sets of basis functions discretizing the two components of the normal stress. To see why this is the case, consider the situation in which Ω is subdivided into Ω_1 and Ω_2; let us denote as always the interface of the two partitions by Γ. Multiplying the momentum equation by a test function $\mathbf{v} \in [H^1_{\Gamma_D}(\Omega)]^2$ and integrating by parts on Ω_1 leads to

$$\mu \int_{\Omega_1} \nabla \mathbf{u} : \nabla \mathbf{v} \, \mathrm{d}\mathbf{x} - \int_{\Omega_1} p \nabla \cdot \mathbf{v} \, \mathrm{d}\mathbf{x} - \int_{\Gamma} \sigma(\mathbf{u}, p)\mathbf{n} \cdot \mathbf{v} \, \mathrm{d}\mathbf{x} = \int_{\Omega_1} \mathbf{f} \cdot \mathbf{v} \, \mathrm{d}\mathbf{x} + \int_{\partial\Omega_1 \cap \Gamma_N} \mathbf{h} \cdot \mathbf{v} \, \mathrm{d}\mathbf{x}.$$

The integral on Γ is the coupling term. Each of the two components of the normal stress $\sigma(\mathbf{u}, p)\mathbf{n}$ must be discretized by a set of basis functions. In this paper, we choose for simplicity to use the same set for the two components of the normal stress.

We consider again Fourier basis functions for the approximation of the normal stresses. Since, as explained in Remark 6.3, we need two Lagrange multipliers for representing each normal stress, the number of basis functions on the ith interface $\Gamma^{(i)}$ is found as $n_\Gamma^{(i)} = 2(2n_{\omega^{(i)}} + 1)$, where $n_{\omega^{(i)}}$ is the number of frequencies. We consider the same number of frequencies on each of the interfaces, *i.e.* $n_\omega \equiv n_{\omega^{(1)}} = n_{\omega^{(2)}} = n_{\omega^{(3)}}$. Therefore, the total number of basis functions for the Lagrange multiplier space is simply given by $n_\Gamma = \sum_{i=1}^3 n_\Gamma^{(i)} = 6(2n_\omega + 1)$. This choice is uniquely made to reduce the number of free parameters and to ease the analysis of the numerical results. Similarly to what noted in Section 6.2.2, where we employed the same number of frequencies in the two parametric directions of the two dimensional interface, one could equally decide to vary the number of basis functions on each interface, if such decision was motivated by the application at hand.

Remark 6.4. The discretized (non-linear) Navier–Stokes equations (6.6) are solved by means of Newton's method with stopping tolerance 10^{-8}. We observe that employing orthogonal basis functions on the interfaces in this context is beneficial because this allows to control the condition number of the Jacobian system. In the numerical simulations we present, however, we were able to obtain the optimal convergences (*i.e.* increase n_Γ as much as required) without orthonormalizing the basis functions of the Lagrange multipliers. The non-linear solver always converged in three iterations or less.

6.3.1. FEM-FEM coupling

We focus on the convergence of the problem when the discrete spaces in the three subdomains are built by means of finite element functions. We define a family of globally non-conforming triangulations $\mathcal{T}^h$ characterized by the mesh size h, namely the maximum edge length over Ω. We remark that, since the exact geometry features curved boundaries, these triangulations are associated to a geometric error; this is not the case when some of the subdomains are discretize by IGA, as in Section 6.3.2. Differently from what done in Section 6.2, we only focus on non-conforming meshes and we exclusively employ the inf-sup stable Taylor-Hood [30] elements with quadratic basis functions for the velocity and linear basis functions for the pressure (which in the following will be denoted P2-P1 basis functions). To compute the error of the solution obtained with the non-conforming method, we consider a reference solution $\mathbf{u}$ obtained with P3-P2 basis functions on a fine conforming mesh ($h_{\text{fine}} = 1.12 \times 10^{-2}$, corresponding to $1'509'020$ and $335'887$ degrees of freedom for the velocity and the pressure respectively).

Figure 10 (*left*) displays the contour lines of the solution corresponding to the mesh size $h = 7.13 \times 10^{-2}$ and $n_\omega = 4$. For this discretization of the Lagrange multiplier space, the contour lines at both sides of each interface match quite accurately and, therefore, the continuity of the global solution is well recovered. Figure 10 (*right*) shows that, if n_Γ is large enough, the following error estimate for P2-P1 elements

$$\left(\sum_{i=1}^3 \|\mathbf{u} - \mathbf{u}^h\|^2_{H^1(\Omega_i)} \right)^{1/2} + \left(\sum_{i=1}^3 \|p - p^h\|^2_{L^2(\Omega_i)} \right)^{1/2} \leq Ch^2 \tag{6.7}$$

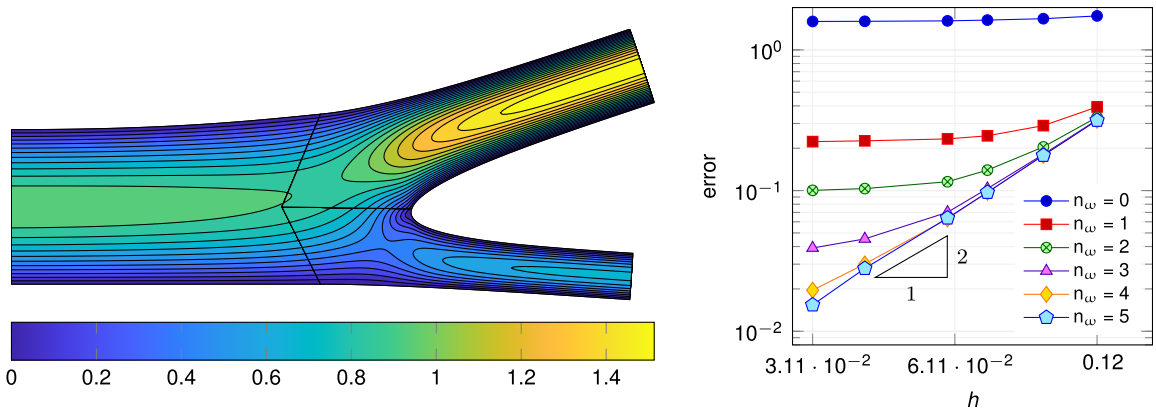

FIGURE 10. *Left panel*: solution of the Navier–Stokes computed on a mesh with size $h = 7.13 \cdot 10^{-2}$ and employing $n_\omega = 4$ frequencies (corresponding to $n_\Gamma = 54$ basis functions for Λ^δ). *Right panel*: convergence of the error (as defined in Eq. (6.7)) with respect to the mesh size h, for different values of n_Γ.

holds. In particular, we observe that when only low frequencies are considered, the error on the Lagrange multiplier λ is larger than the finite element error and the global error remains approximately constant when h tends to zero. For $n_\omega = 4$ and $n_\omega = 5$, on the other hand, the error on λ is negligible and the rate of convergence of FEM is fully recovered. We remark that, compared to the total number of degrees of freedom for velocity and pressure in the three subdomains – which ranges in the intervals $3'232-48'978$ for Ω_1, $1'463-39'080$ for Ω_2 and $2'760-93'202$ for Ω_3 – the number of basis functions of Λ^δ considered in Figure 10 (*right*) is negligible (we take at most $n_\Gamma = 66$).

Figure 11 shows the distribution of the error $|\mathbf{u} - \mathbf{u}^h|$ on the domain Ω on two non-conforming meshes, when different numbers of frequencies are considered. Note that, being the color scale logarithmic, we set the error on the Dirichlet boundaries (which is zero) to the arbitrary value 10^{-16}. In the first two rows, corresponding to the choice $n_\omega = 0$ (*top row*) and $n_\omega = 2$ (*middle row*), the error is mostly concentrated in correspondence of the interfaces (in particular Γ_2) and the maximum values reached for the two different mesh sizes are similar; this effect is caused by the poor approximation of the Lagrange multiplier spaces. In the bottom row, instead, the maximum values of the error reached on the finer mesh are significantly smaller than those obtained on the coarser mesh. Moreover, on the coarse mesh the error is not localized in correspondence of any interface (that is, the finite element error dominates the error on the Lagrange multiplier reconstruction), whereas on the finer mesh the larger errors are still found in correspondence of Γ_2.

6.3.2. FEM-IGA coupling

We now investigate the possibility of coupling different numerical schemes by spectral Lagrange multipliers. Specifically, we consider IGA for the discretization of Ω_1 and Ω_3, and FEM for the discretization of Ω_2.

For the sake of conciseness, we do not focus on the details of IGA and we limit ourselves to recall the general ideas of the method. The interested reader is referred to *e.g.* [21,31] for a complete overview, and to [16] for an application of the mortar method to IGA.

IGA is built upon the isoparametric concept, which prescribes the use of the same basis functions for the geometry generation and the discretization of the functional spaces where the solution of the differential problem is sought in. The most common choices for such basis functions are B-Splines and NURBS (Non-Uniform Rational B-Splines), which are commonly employed in all modern CAD (Computer-Aided Design) software. In this work, we solely focus on B-Splines, which are sufficient to represent the bifurcation in Figure 9. The principal advantages of the approach are: (i) the global high continuity of the basis functions, which often entails higher

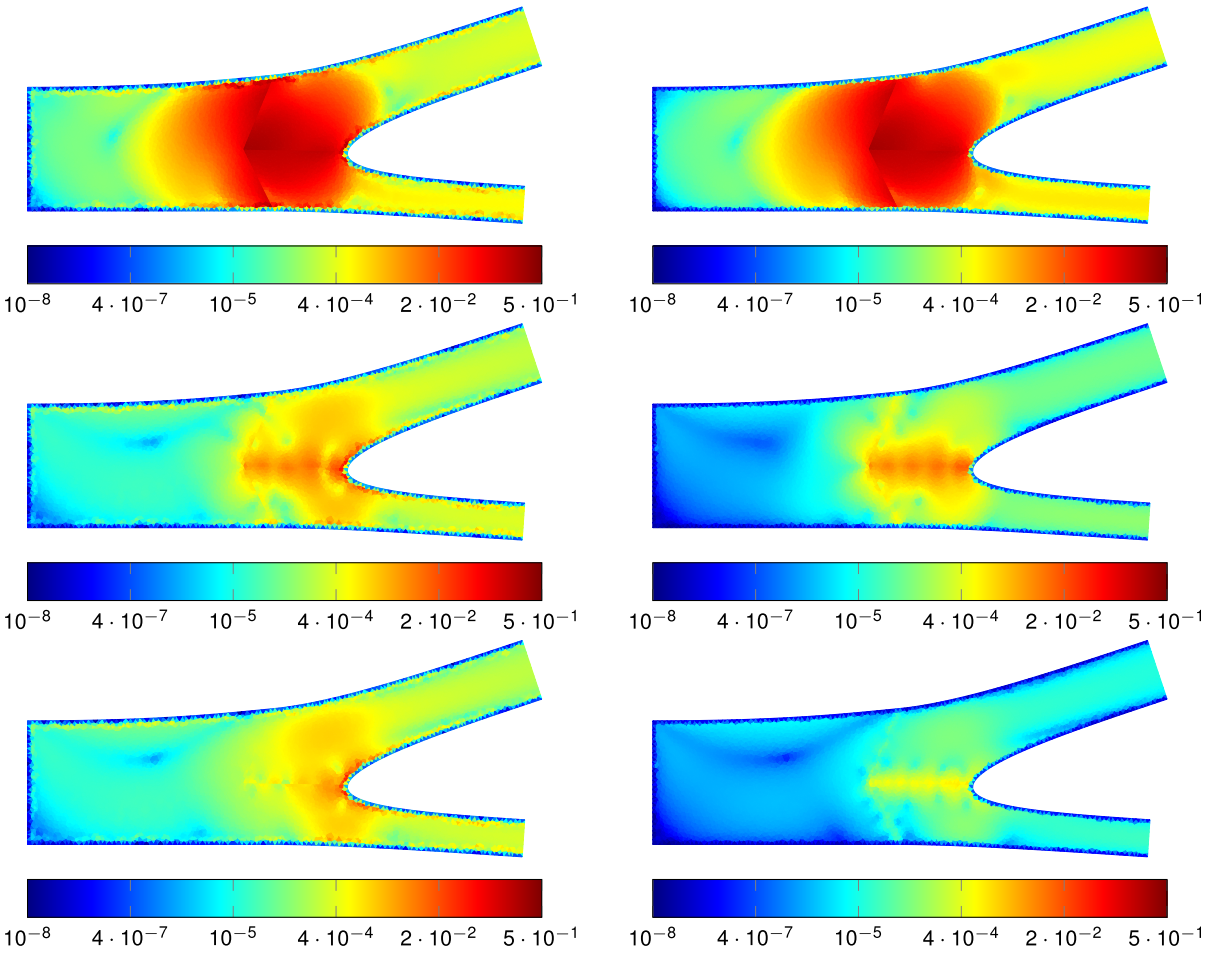

(A) $h = 9.29 \cdot 10^{-2}$ (B) $h = 3.11 \cdot 10^{-2}$

FIGURE 11. Error distribution on the bifurcation when employing $n_\omega = 0$ (*top row*), $n_\omega = 2$ (*middle row*) and $n_\omega = 4$ (*bottom row*) and a coarse mesh (*left column*, $h = 9.29 \cdot 10^{-2}$) and a fine mesh (*right column*, $h = 3.11 \cdot 10^{-2}$).

accuracy than standard finite elements functions with equal polynomial degree (which are only C^0- continuous across the edges of the mesh), and (ii) the exact correspondence of geometry and computational domain, that is, the method does not require any mesh generation and – consequently – no geometrical approximation of curved boundaries.

Univariate B-Splines basis functions of order p are generated by means of the Cox-De Boor recursion formula [22] from a knot vector $\Xi = [\xi_1, \ldots, \xi_{n+p+1}]$; we remark that we decided to adopt the usual notation ξ_i commonly found in the literature to denote the individual knots, even though we previously associated such letter to the basis functions of Λ^δ. In this paper we consider open knot vectors, *i.e.* knot vectors such that $\xi_1 = \ldots = \xi_{p+1}$ and $\xi_{n+1} = \ldots = \xi_{n+p+1}$. The continuity of the basis functions across each internal knot ξ_i is determined by its multiplicity, *i.e.* the continuity of the basis functions across such point is C^{p-m_i}. Multivariate B-Splines are obtained by the tensor product of two sets of univariate B-Splines. In the following, we will denote $\{\widehat{\varphi}_i\}_{i=1}^{n_{\text{bf}}}$ a set of bivariate basis functions; note that, as the polynomial degrees in the two parametric dimensions is *a priori*

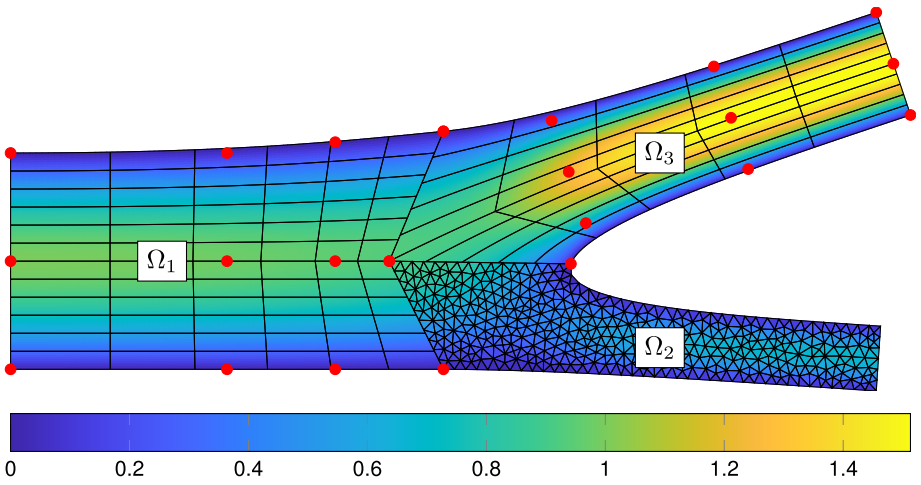

FIGURE 12. Global solution obtained by considering 6×12 elements and P3-P2 B-Spines basis functions in Ω_1, a finite element mesh with size $h = 7.16 \cdot 10^{-2}$ and P2-P1 basis functions in Ω_2, 5×10 elements and P3-P2 B-Splines basis functions in Ω_3, and $n_\omega = 5$ frequencies for the discretization of Λ^δ. The control points are marked with red dots.

different, we omit to specify the degree of the bivariate polynomials. Moreover, we introduce the parametric domain $\widehat{\Omega} \in \mathbb{R}^2$, which is the support of the bivariate functions.

B-Splines surfaces are obtained from bivariate B-Splines by means of their linear combination with control points $\{\mathbf{b}_i\}_{i=1}^{i=n}$, where each $\mathbf{b}_i$ belongs either to $\mathbb{R}^2$ or to $\mathbb{R}^3$ if the surface is embedded in two or three dimensions respectively (here, we consider the former case). Therefore, the function

$$\mathbf{x}(\widehat{\mathbf{x}}) = \sum_{i=1}^{n_{\text{bf}}} \widehat{\varphi}_i(\widehat{\mathbf{x}})\mathbf{b}_i : \widehat{\Omega} \to \Omega \tag{6.8}$$

defines a mapping – which we assume invertible for all $\widehat{\mathbf{x}} \in \widehat{\Omega}$ – from the parametric space $\widehat{\Omega}$ to the physical space Ω. By the isoparametric concept, we define a set of basis functions on Ω as $\varphi_i = \widehat{\varphi}_i \circ \mathbf{x}^{-1}$, for all $i = 1, \ldots, n_{\text{bf}}$. We remark that the resulting functional space, even if intrinsically linked to the geometry definition, can be enriched by knot insertion (h-refinement), order elevation (p-refinement) and a combination of the two techniques (k-refinement) [20]; such modifications of the knot vectors in the parametric dimensions do not affect the geometry of the physical domain.

Figure 12 shows as an example the partitioned domain Ω with a finite element triangulation in Ω_2 and a subdivision into elements of the physical domains Ω_1 and Ω_3. These are obtained from mappings of the form (6.8), acting from the parametric domains $\widehat{\Omega}_1 = \widehat{\Omega}_3 = [0, 0, 0, 0, 1, 1, 1, 1] \times [0, 0, 0.5, 1, 1]$. The resulting bivariate space is then composed of P3/C2 (piecewise cubic with continuity up to the second derivatives) basis functions in the first direction, and P1/C0 (piecewise linear with C^0-continuity) basis functions. The corresponding control points are marked with red dots.

In order to approximate the two components of the velocity and the pressure appearing in the Navier–Stokes equations, we define functional spaces as presented above. In particular, in Ω_1 and Ω_2 we employ Taylor-Hood elements – which, in the context of IGA, have been analyzed *e.g.* in [17] – of degree p and continuity $p - 1$ for the pressure and degree $p + 1$ and continuity p for the velocity, whereas in Ω_2 we only consider P2-P1 basis functions. A global solution obtained by using P3-P2 basis functions in Ω_1, P2-P1 basis functions in Ω_2 and P2-P1 basis functions in Ω_3 is shown in Figure 12.

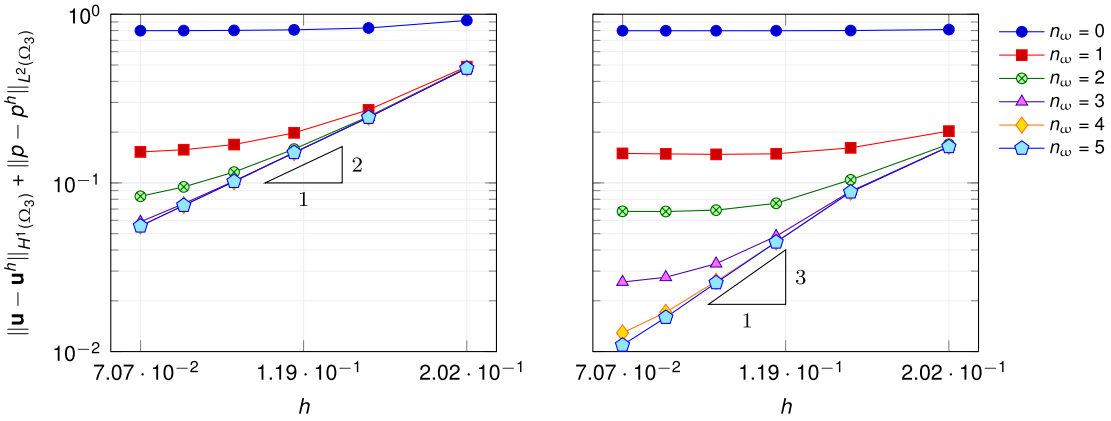

FIGURE 13. Convergence of the error in Ω_3 with respect to the mesh size h and number of basis functions on the interface n_Γ. The basis functions in Ω_3 are P2-P1 B-Splines (*left panel*) and P3-P2 (*right panel*).

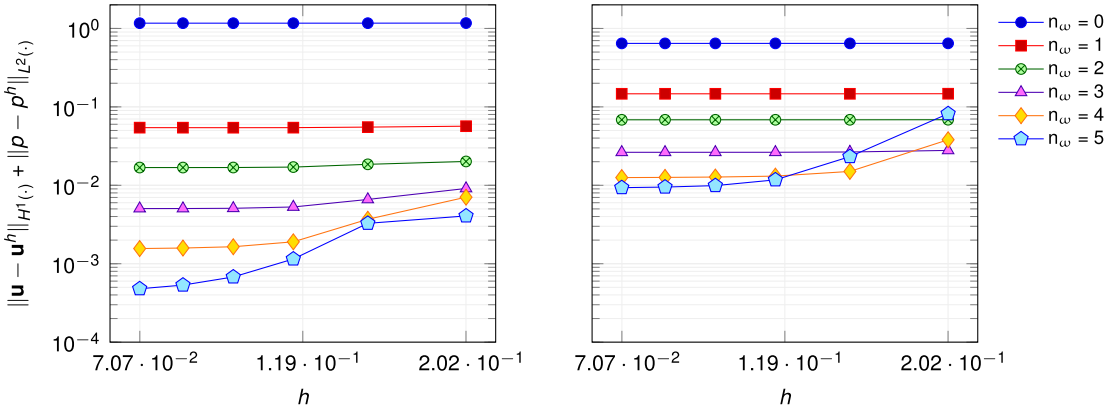

FIGURE 14. Error in Ω_1 (*left panel*) and Ω_2 (*right panel*) with respect to the mesh size h in Ω_3. In the latter subdomain, we employ P3-P2 B-Splines basis functions.

In this simulation, we test the convergence of the error with respect to the mesh size of a single subdomain, namely Ω_3. To this end, we fix the number of degrees of freedom in Ω_1 and Ω_2 and progressively refine the mesh in Ω_3. In Ω_1, we employ P3-P2 basis functions and 3'200 elements, for a total of 27'390 and 3'655 degrees of freedom for the velocity and the pressure respectively; in Ω_2 we consider P2-P1 finite element basis functions on a mesh with 12'448 elements, which correspond to 50'590 and 12'848 degrees of freedom for the velocity and the pressure respectively. Figure 13 shows the convergence of the error with respect to the mesh size in Ω_3, for various levels of discretization of the space Λ^δ, when P2-P1 (on the left) and P3-P2 (on the right) Taylor-Hood basis functions are employed. The error is computed with respect to the fine finite element solution obtained with P3-P2 basis functions we already considered in Section 6.3.1. The results are consistent with what found in the previous sections, and in both cases we are able to recover the optimal convergence of IGA (quadratic on the left, cubic on the right). Figure 14 shows the behavior of the error in the first two subdomains when P3-P2 basis functions are employed in Ω_3 on a mesh with varying size. These results show that the accuracy of the stress reconstruction at the interfaces has a strong impact on the accuracy of the solution in Ω_1 and Ω_2. Smaller meshes sizes in Ω_3 together with good approximation of the Lagrange multipliers, indeed, lead to

smaller errors in the two subdomains even if the number of degrees of freedom of the respective local solutions remains constant.

7. Conclusions

We presented a non-conforming method for the coupling of PDEs defined on domains partitioned into non-overlapping subdomains. At the continuous level, our method and the mortar method are based on the same weak formulations in which the continuity constraints over the primal (the solution) and the dual (the stress) variables are enforced via Lagrange multipliers. As we described in the paper, our choice of discretizing the space of Lagrange multipliers independently of the spatial discretization in the subdomains offers the advantage of a straight-forward implementation of the method and the possibility of tuning the accuracy of the coupling as required by the application; we limited ourselves to considering Fourier basis functions defined over the interface. However, the saddle-point nature of the problem poses constraints over the richness of the discretized space for the Lagrange multipliers compared to the degrees of freedom of the primal variable: we empirically verified that the inf-sup constant can be controlled dependently on the mesh size, in the sense that finer meshes allow considering larger number of Fourier basis functions, without violating the inf-sup stability. In the numerical experiments, we showed that the optimal convergence of the finite element method was recovered for the Poisson problem; this was confirmed both when using conforming and non-conforming meshes, and when using different polynomial degrees in the subdomains. We also verified that the error obtained when employing a sufficiently rich basis for the Lagrange multiplier spaces is equal to that obtained considering a global conforming mesh with comparable size (see Fig. 4). Since this represents a lower bound for the error of the mortar method as well, it can be said that – with an appropriate choice of basis functions for the Lagrange multiplier space – our method performs at least as well as the mortar method in terms of accuracy. In the last part of the paper, we showed that the method can be easily extended to the case of non-elliptic equations, such as the Navier–Stokes equations, and to cases in which multiple partitions of the domain are discretized with different numerical methods, namely the finite element method and isogeometric analysis. Also in these numerical simulations were able to retain optimal convergence rates by choosing an appropriate number of basis functions for the approximation of the Lagrange multiplier space.

We described a coupling strategy based on classical results that showed desirable convergence properties and we were able to apply such technique to a variety of non-conforming approximations of PDEs. Nevertheless, there are still matters that need to be addressed. We believe that future improvements of the current work should discuss, in particular, (i) the development of *a priori* estimates for the optimal choice of n_Γ, (ii) the theoretical analysis of the conditioning of the system arising from the coupling in terms of number of basis functions for the Lagrange multiplier space, of their orthonormality, and the number of considered subdomains, and (iii) the design of ad-hoc preconditioners for the saddle-point linear system.

Acknowledgements. The authors are grateful to Prof. Annalisa Buffa and Prof. Alfio Quarteroni for the fruitful discussions and their advice on the topics presented in this paper, and Dr. Rafael Vázquez and Luca Coradello for their support with GeoPDEs. The research of the authors is supported by the Swiss National Foundation (SNF), project No. 200021E-168311. The authors acknowledge the anonymous referees whose criticism and recommendations have stimulated the improvement of the original version of the paper.

References

[1] S.K. Acharya and A. Patel, Primal hybrid method for parabolic problems. *Appl. Numer. Math.* **108** (2016) 102–115.

[2] F. Ballarin, A. Manzoni, A. Quarteroni and G. Rozza, Supremizer stabilization of POD–Galerkin approximation of parametrized steady incompressible Navier–Stokes equations. *Int. J. Numer. Methods Eng.* **102** (2015) 1136–1161.

[3] R. Becker, P. Hansbo and R. Stenberg, A finite element method for domain decomposition with non-matching grids. *ESAIM: M2AN* **37** (2003) 209–225.

[4] F.B. Belgacem, The mortar finite element method with Lagrange multipliers. *Numer. Math.* **84** (1999) 173–197.

[5] F.B. Belgacem, L.K. Chilton and P. Seshaiyer, The hp-mortar finite-element method for the mixed elasticity and stokes problems. *Comput. Math. App.* **46** (2003) 35–55.
[6] C. Bernardi, A new nonconforming approach to domain decomposition: the mortar element method. *Nonlinear Partial Equ. App.* (1989).
[7] C. Bernardi, Y. Maday and F. Rapetti, Basics and some applications of the mortar element method. *GAMM-Mitteilungen* **28** (2005) 97–123.
[8] L. Bertagna, S. Deparis, L. Formaggia, D. Forti and A. Veneziani, The LifeV library: engineering mathematics beyond the proof of concept. Preprint arXiv:1710.06596 (2017).
[9] D. Boffi, F. Brezzi and M. Fortin, Mixed Finite Element Methods and Applications. Springer, Berlin **44** (2013).
[10] Z. Bontinck, J. Corno, S. Schöps and H. De Gersem, Isogeometric analysis and harmonic stator–rotor coupling for simulating electric machines. *Comput. Methods Appl. Mech. Eng.* **334** (2018) 40–55.
[11] D. Braess, W. Dahmen and C. Wieners, A multigrid algorithm for the mortar finite element method. *SIAM J. Numer. Anal.* **37** (1999) 48–69.
[12] F. Brezzi, On the existence, uniqueness and approximation of saddle-point problems arising from lagrangian multipliers. *Rev. Fr. Autom. Inform. Rech. Opér. , Anal. Numér.* **8** (1974) 129–151.
[13] F. Brezzi and K.-J. Bathe, A discourse on the stability conditions for mixed finite element formulations. *Comput. Methods Appl. Mech. Eng.* **82** (1990) 27–57.
[14] F. Brezzi and D. Marini, Error estimates for the three-field formulation with bubble stabilization. *Math. Comput.* **70** (2001) 911–934.
[15] F. Brezzi and L.D. Marini, A three-field domain decomposition method. *Contemp. Math.* **157** (1994) 27–34.
[16] E. Brivadis, A. Buffa, B. Wohlmuth and L. Wunderlich, Isogeometric mortar methods. *Comput. Methods Appl. Mechan. Eng.* **284** (2015) 292–319.
[17] A. Buffa, C. De Falco and G. Sangalli, Isogeometric analysis: stable elements for the 2D Stokes equation. *Int. J. Numer. Methods Fluids* **65** (2011) 1407–1422.
[18] J. Céa, Approximation variationnelle des problèmes aux limites. *Ann. Inst. Fourier (Grenoble)* **14** (1964) 345–444.
[19] P.G. Ciarlet, The Finite Element Method for Elliptic Problems. SIAM, Philadelphia (2002).
[20] J. Cottrell, T. Hughes and A. Reali, Studies of refinement and continuity in isogeometric structural analysis. *Comput. Methods Appl. Mech. Eng.* **196** (2007) 4160–4183.
[21] J.A. Cottrell, T.J. Hughes and Y. Bazilevs, Isogeometric Analysis: Toward Integration of CAD and FEA. John Wiley & Sons, Hoboken, NJ (2009).
[22] C. De Boor, On calculating with B-splines. *J. Approx. Theor.* **6** (1972) 50–62.
[23] S. Deparis, M. Discacciati and A. Quarteroni, A domain decomposition framework for fluid-structure interaction problems. *Comput. Fluid Dyn. 2004* (2006) 41–58.
[24] S. Deparis, D. Forti and A. Quarteroni, A rescaled localized radial basis function interpolation on non-cartesian and nonconforming grids. *SIAM J. Sci. Comput.* **36** (2014) A2745–A2762.
[25] S. Deparis, D. Forti, P. Gervasio and A. Quarteroni, INTERNODES: an accurate interpolation-based method for coupling the Galerkin solutions of PDEs on subdomains featuring non-conforming interfaces. *Comput. Fluids* **141** (2016) 22–41.
[26] A. Ehrl, A. Popp, V. Gravemeier and W. Wall, A dual mortar approach for mesh tying within a variational multiscale method for incompressible flow. *Int. J. Numer. Methods Fluids* **76** (2014) 1–27.
[27] D. Forti, *Parallel algorithms for the solution of large-scale fluid-structure interaction problems in hemodynamics*. Ph.D. thesis, EPFL (2016).
[28] V. Girault and P.-A. Raviart, Finite Element Methods for Navier–Stokes Equations: Theory and Algorithms. Springer Science & Business Media, Berlin **5** (2012).
[29] C. Hesch, A. Gil, A.A. Carreño, J. Bonet and P. Betsch, A mortar approach for fluid–structure interaction problems: immersed strategies for deformable and rigid bodies. *Comput. Methods Appl. Mech. Eng.* **278** (2014) 853–882.
[30] P. Hood and C. Taylor, Navier–Stokes equations using mixed interpolation. *Finite Elem. Methods Flow Prob.* (1974) 121–132.
[31] T.J. Hughes, J.A. Cottrell and Y. Bazilevs, Isogeometric analysis: CAD, finite elements, NURBS, exact geometry and mesh refinement. *Comput. Methods Appl. Mech. Eng.* **194** (2005) 4135–4195.
[32] M. Israeli, L. Vozovoi and A. Averbuch, Domain decomposition methods for solving parabolic PDEs on multiprocessors. *Appl. Numer. Math.* **12** (1993) 193–212.
[33] T. Klöppel, A. Popp, U. Küttler and W.A. Wall, Fluid-structure interaction for non-conforming interfaces based on a dual mortar formulation. *Comput. Methods Appl. Mech. Eng.* **200** (2011) 3111–3126.
[34] A. Popp and W. Wall, Dual mortar methods for computational contact mechanics–overview and recent developments. *GAMM-Mitteilungen* **37** (2014) 66–84.
[35] M.A. Puso, A 3D mortar method for solid mechanics. *Int. J. Numer. Methods Eng.* **59** (2004) 315–336.
[36] M.A. Puso and T.A. Laursen, A mortar segment-to-segment contact method for large deformation solid mechanics. *Comput. Methods Appl. Mech. Eng.* **193** (2004) 601–629.
[37] A. Quarteroni, Numerical Models for Differential Problems. Springer-Verlag **8** (2014).
[38] A. Quarteroni and A. Valli, Domain decomposition methods for partial differential equations. *Numerical Mathematics and Scientific Computation*. Oxford University Press, Oxford (1999).
[39] A. Quarteroni and A. Valli, Numerical Approximation of Partial Differential Equations. In Vol. 23 of Springer Series in Computational Mathematics Springer-Verlag Berlin Heidelberg (1994).

[40] P.-A. Raviart and J. Thomas, Primal hybrid finite element methods for 2nd order elliptic equations. *Math. Comput.* **31** (1977) 391–413.

[41] A. Ruhe, Numerical aspects of Gram-Schmidt orthogonalization of vectors. *Linear Algebra App.* **52** (1983) 591–601.

[42] S. Salsa, Partial Differential Equations in action: from modelling to theory. In Vol. 99. Springer, Berlin (2016).

[43] P. Seshaiyer, Stability and convergence of nonconforming hp finite-element methods. *Comput. Math. App.* **46** (2003) 165–182.

[44] P. Seshaiyer and M. Suri, Convergence results for non-conforming hp methods: The mortar finite element method. *Contemp. Math.* **218** (1998) 453–459.

[45] A. Toselli and O.B. Widlund, Domain decomposition methods: algorithms and theory. In Vol. 34 of *Springer Series in Computational Mathematics*. Springer, Berlin (2005).

[46] R. Vázquez, A new design for the implementation of isogeometric analysis in Octave and Matlab: GeoPDEs 3.0. *Comput. Math. App.* **72** (2016) 523–554.

[47] B.I. Wohlmuth, A mortar finite element method using dual spaces for the Lagrange multiplier. *SIAM J. Numer. Anal.* **38** (2000) 989–1012.